Tidal Evolution of the Uranian Satellites

II. An Explanation of the Anomalously High Orbital Inclination of Miranda

WILLIAM C. TITTEMORE[1] AND JACK WISDOM

Department of Earth, Atmospheric, and Planetary Sciences, Massachusetts Institute of Technology, Cambridge, Massachusetts 02139

Miranda and Umbriel have passed through the 3:1 mean-motion commensurability if the specific dissipation function (Q) of Uranus is less than about 39,000. There are three second-order inclination resonances associated with this commensurability. Temporary capture into either of the resonances involving the orbital inclination of Miranda can account for the anomalously high (~4°) current inclination of Miranda. As the satellites approach the commensurability at low orbital inclinations, the coupling between the resonances is very weak, and capture into either of the resonances involving the orbital inclination of Miranda is likely. The evolution of the system after capture into one of these resonances is initially described well by the standard theory of evolution through isolated mean-motion resonances. However, as the orbital inclination of Miranda increases, and the coupling between the resonances becomes stronger, the separatrices associated with the resonances broaden into chaotic zones and eventually merge, creating a sizable chaotic region. Escape from resonance occurs via a qualitatively new dynamical mechanism. The trajectory encounters low-order commensurabilities between the libration frequency of the resonant argument and other fundamental frequencies in the system. If the trajectory is captured into any of these secondary resonances, it is dragged into the chaotic region, whereupon the system can escape the mean-motion commensurability. Miranda retains a high orbital inclination comparable to the current value. Since the anomalously large inclination of Miranda is a natural outcome of passage through the 3:1 commensurability, the requirement that the satellites have encountered this resonance constrains the Q of Uranus to be less than 39,000. © 1989 Academic Press, Inc.

1. INTRODUCTION

Some of the dynamical properties of the Uranian satellite system, such as the anomalously high orbital inclination of Miranda and the anomalously high orbital eccentricities of the inner large satellites, cannot be explained by the current interactions between the satellites (Dermott and Nicholson 1986, Laskar 1986), and therefore suggest origins in past dynamical interactions. In addition, the relatively young

[1] Now at the Department of Planetary Sciences, Lunar and Planetary Laboratory, University of Arizona, Tucson, AZ 85721.

surfaces of Miranda and Ariel (Smith *et al.* 1986) suggest that tidal heating may have been important in the thermal histories of these satellites. If the orbits of the satellites have evolved significantly due to tidal friction, they may have passed through low-order mean-motion commensurabilities. We are investigating the past resonant interactions of the satellites to determine if they can account for the above observations, as well as allowing the satellite system to reach its present nonresonant configuration.

In cases where the motion near a resonance is dominated by the perturbations of a single resonant argument, for instance,

63

where the resonances near a mean-motion commensurability are well separated by a large planetary oblateness, the dynamics can be described by the standard integrable theory of evolution through resonances (Goldreich and Peale 1966, Counselman and Shapiro 1970, Yoder 1979, Henrard 1982, Henrard and Lemaitre 1983, Borderies and Goldreich 1984, Lemaitre 1984). However, in cases where there are many essential contributions to the motion near a resonance, for example, where there is a significant coupling between resonances and/or a strong secular interaction, the assumptions made in deriving the single-resonance formulae may not apply. Specifically, the motion in a relatively large region of phase space near the separatrix at a resonance may be chaotic and therefore nonintegrable. In the Uranian system, where the satellite-to-planet mass ratios are relatively high and the planetary oblateness is small, there are significant chaotic zones at the resonances.

The authors (Tittemore and Wisdom 1988, henceforth referred to as Paper I) have studied the most recently encountered of these resonances, the 5 : 3 commensurability involving Ariel and Umbriel, and have found that the presence of a large chaotic zone significantly affects the mechanisms and outcomes of resonance passage. It is expected that other resonances in the Uranian system will show chaotic behavior, since the same conditions of small J_2 and strong secular coupling apply. We have found this to be the case in the Miranda–Umbriel 3 : 1 mean-motion commensurability, which is a second-order resonance with properties similar to those of the 5 : 3 resonance. In particular, the anomalously high current inclination of Miranda can be explained as a result of passage through this commensurability.

In Section 2, the resonant Hamiltonian is discussed. We begin by studying the circular-inclined approximation, in order that we may attempt to gain some understanding of the dynamics of the 3 : 1 mean-motion reso-

nance that are relevant to the evolution of the inclinations of the orbits of these two satellites. The circular-inclined Hamiltonian can be reduced to two degrees of freedom, allowing us to study the phase space of the problem in detail, using the Poincaré surface of section technique.

In Paper I, the authors discovered that the simulated rate of tidal evolution through the Uranian resonances must be extremely slow ($\dot{a}/a < 10^{-10}$ per orbit period) to avoid rate-induced dynamical artifacts. At such slow orbital expansion rates, it is necessary to integrate the equations of motion of order 10^8 orbit periods to properly explore the evolution of satellites through a mean-motion commensurability. Using classical integration techniques for this purpose would require prohibitively large amounts of computer time. The algebraic mapping technique for integrating orbital equations, first developed by Wisdom (1982, 1983) for the study of resonant asteroid motion, provides a method with which the evolution through a mean-motion commensurability may be explored with reasonable amounts of computer time. A mapping for second-order resonant motion involving two satellites of comparable mass was developed in Paper I, and has been employed for the calculations presented here.

Numerical integrations of the evolution through this commensurability (Section 3) reveal very interesting behavior. As the satellites approach the commensurability at low inclinations, the system behaves as if the resonances are isolated, with a significant probability of capture into either of the second-order resonances involving the orbital node of Miranda. Following capture into one of these resonances, the evolution of the system is temporarily quasiperiodic. The trajectory occupies a region of phase space in which one of the resonant arguments involving the orbital node of Miranda librates, and the evolution can initially be described well by the single-resonance theory. However, as the orbital inclination of Miranda increases, the separatrix associ-

ated with the resonance broadens into a sizable chaotic zone. Large-scale chaos ensues after the separatrices of the individual second-order resonances merge. The onset of large-scale chaos is well predicted by the resonance overlap criteria. The presence of a large chaotic region does not by itself guarantee that the trajectory will become chaotic, though, since the chaotic zone does not fully engulf the libration regions. However, there is another dynamical mechanism at work in this system. As the system evolves within one of the resonances, the frequency of small-amplitude libration of the resonant argument increases. The system encounters low-order commensurabilities between the libration frequency and other fundamental frequencies. These form a secondary resonant structure in the pendulum-like phase space of this dynamical system. If the system is captured into one of these secondary resonances, the trajectory is eventually "dragged" away from the center of the libration region and into the large chaotic zone, and the system can escape from the primary resonance, with the orbit of Miranda retaining a relatively high inclination comparable to its current value. The results of our numerical experiments agree well with analytic predictions of the width of the chaotic separatrix, the onset of large-scale chaos accompanying the overlap of primary resonance regions, and the locations of the secondary resonances between degrees of freedom in this problem.

In Sections 4 and 5, the investigation of this resonance is generalized to include other dynamical perturbations occurring in the Uranian satellite system. We investigate the effects of the eccentricity-type resonances, and the effects of the secular interactions between Ariel and the satellites involved in the inclination resonances. The interesting mechanisms found in the circular-inclined problem are present in both of these models—the orbital inclination of Miranda still jumps to a high value before the system escapes from the resonance.

The final section discusses the implications of our results for the Uranian system. Passage through the Miranda–Umbriel 3 : 1 commensurability provides a convincing mechanism by which Miranda attained its present anomalously high orbital inclination. Thus the requirement that the system encountered this resonance can be used to constrain the specific dissipation function (Q) of Uranus to be less than 39,000.

2. THE RESONANT HAMILTONIAN

In this paper, we consider the interaction between Miranda and Umbriel near the 3 : 1 mean-motion commensurability, which involves three second-order inclination resonances and three second-order eccentricity resonances. The spherical harmonic J_2 of Uranus is small, so the resonances cannot be considered individually. Since the resonant and secular interactions take place on timescales which are generally much longer than the orbit periods, we average over high-frequency contributions involving nonresonant combinations of the mean longitudes. The masses of the two satellites are within about an order of magnitude of each other, so the orbits of both satellites will be influenced by the interaction. In this section, we consider the circular-inclined problem as a first approximation to the resonant evolution of the inclinations of Miranda and Umbriel. This reduces to a two degree of freedom problem, similar to the planar eccentric problem developed in Paper I for the Ariel–Umbriel 5 : 3 resonance, which is of second order in eccentricities. The development of the Hamiltonian is very similar in both cases, and we refer the reader to Appendix I of Paper I for a more formal development of a second-order resonant Hamiltonian than is described here. The subscript M refers to Miranda and the subscript U to Umbriel in the following development of the Hamiltonian.

Expressing the contributions to the Hamiltonian in terms of Keplerian elements, where a_i is the semimajor axis, i_i is the incli-

nation, λ_i is the mean longitude, and Ω_i is the longitude of perihelion, the Keplerian contribution to the motion is

$$\mathcal{H}_K = -\frac{GMm_M}{2a_M} - \frac{GMm_U}{2a_U}. \quad (1)$$

Keeping only the J_2 terms to second order in inclination in the expression of the potential for an oblate planet,

$$\mathcal{H}_O = -\frac{GMm_M}{2a_M} J_2 \left(\frac{R}{a_M}\right)^2 \left[1 - \frac{3}{2}i_M^2\right]$$
$$- \frac{GMm_U}{2a_U} J_2 \left(\frac{R}{a_U}\right)^2 \left[1 - \frac{3}{2}i_U^2\right], \quad (2)$$

and from the expression for the disturbing function (Leverrier 1855), the secular contribution is

$$\mathcal{H}_S = -\frac{Gm_M m_U}{a_U} \left[(1)^{(0)} + (11)^{(0)} \left\{\left(\frac{i_M}{2}\right)^2\right.\right.$$
$$\left.\left. + \left(\frac{i_U}{2}\right)^2 - 2.0 \frac{i_M}{2} \frac{i_U}{2} \cos(\Omega_M - \Omega_U)\right\}\right] \quad (3)$$

and the resonant contribution is

$$\mathcal{H}_R = -\frac{Gm_M m_U}{a_U} (212)^{(3)}$$
$$\times \left[\left(\frac{i_M}{2}\right)^2 \cos(3\lambda_U - \lambda_M - 2\Omega_M)\right.$$
$$- 2.0 \frac{i_M}{2} \frac{i_U}{2} \cos(3\lambda_U - \lambda_M - \Omega_M - \Omega_U)$$
$$\left. + \left(\frac{i_U}{2}\right)^2 \cos(3\lambda_U - \lambda_M - 2\Omega_U)\right], \quad (4)$$

where

$$(1)^{(0)} = \tfrac{1}{2}b_{1/2}^0(\alpha)$$
$$(11)^{(0)} = -\tfrac{1}{2}\alpha b_{3/2}^1(\alpha)$$
$$(212)^{(3)} = \tfrac{1}{2}\alpha b_{3/2}^2(\alpha) \quad (5)$$

and α is the ratio of semimajor axes, and $b_s^j(\alpha)$ are Laplace coefficients.

We choose as resonance coordinates

$$\sigma_M = \tfrac{1}{2}(3\lambda_U - \lambda_M - 2\Omega_M)$$
$$\sigma_U = \tfrac{1}{2}(3\lambda_U - \lambda_M - 2\Omega_U), \quad (6)$$

which with the mean longitudes λ_M and λ_U form a complete set of canonical variables

for our problem. In terms of the Delaunay momenta $L_i \approx m_i\sqrt{GMa_i}$ and $H_i = L_i \cos(i_i)$, the momenta conjugate to σ_M and σ_M are

$$\Sigma_M = L_M - H_M$$
$$\Sigma_U = L_U - H_U \quad (7)$$

The momenta conjugate to $\gamma_M = \lambda_M$ and $\gamma_U = \lambda_U$,

$$\Gamma_M = L_M + \tfrac{1}{2}(\Sigma_M + \Sigma_U)$$
$$\Gamma_U = L_U - \tfrac{3}{2}(\Sigma_U + \Sigma_U), \quad (8)$$

are integrals of the motion, since we are averaging over motion on timescales of the orbit periods. Note that $\Sigma_i \approx \Gamma_i i_i^2/2$.

The Hamiltonian is expanded in powers of Σ_i/Γ_i to order $m_i^2 i_i^2$, resulting in

$$\mathcal{H} = 2A(\Sigma_M + \Sigma_U) + 4B(\Sigma_M + \Sigma_U)^2$$
$$+ 2C\Sigma_M + 2D\Sigma_U$$
$$+ 2E\sqrt{\Sigma_M\Sigma_U} \cos(\sigma_M - \sigma_U)$$
$$+ 2F\Sigma_M \cos(2\sigma_M)$$
$$+ 2G\sqrt{\Sigma_M\Sigma_U} \cos(\sigma_M + \sigma_U)$$
$$+ 2H\Sigma_U \cos(2\sigma_U). \quad (9)$$

The expressions for the coefficients $A - H$ are given in Appendix 1.

For low inclinations, $A \approx \tfrac{1}{4}(3n_U - n_M)$. Because of the differential expansion of the orbits due to tidal dissipation in Uranus, n_M decreases relative to n_U, and $A \approx 0$ where the mean motions are exactly commensurate. We define the parameter in the problem, δ, to be the angle-independent contributions to $3n_U - n_M - \dot{\Omega}_M - \dot{\Omega}_U$, or $4A + 2(C + D)$. It provides us with a measure of distance from the resonance, and changes sign in the middle of the resonance region. During resonance passage, the fractional change in δ, proportional to the fractional change in A, is much larger than the fractional changes in the other coefficients, which are proportional to changes in the semimajor axis ratio as it appears in the Leverrier coefficients. We therefore ignore changes in the coefficients other than A.

The units chosen are as follows: distance is measured in units of the radius of Uranus R, mass is measured in units of the mass of

Uranus M, and time is measured in years. In these units, the masses of Miranda and Umbriel are, respectively, $m_M = 8.6 \times 10^{-7}$ and $m_U = 1.47 \times 10^{-5}$ (Stone and Miner 1986). The coefficients were evaluated at $\delta = 0$ for $i_i = 0$ and $a_U = 10.1179R$ (the value of the semimajor axis of Umbriel at which the resonance was encountered), which corresponds to $a_M = 4.8645$. The numercial values for the coefficients thus obtained are (see Appendix I): $B = -5167.54$, $C = 0.043832$, $D = -0.121057$, $E = -0.0006756$, $F = -0.0009765$, $G = 0.0003934$, and $H = -0.00003961$. For these physical parameters, the integrals of motion are $\Gamma_M = 0.033946$ and $\Gamma_U = 0.836831$.

In terms of the Cartesian coordinates

$$y_i = \sqrt{2\Sigma_i} \sin(\sigma_i) \approx i_i\sqrt{\Gamma_i} \sin(\sigma_i) \quad (10)$$

and the conjugate momenta

$$x_i = \sqrt{2\Sigma_i} \cos(\sigma_i) \approx i_i\sqrt{\Gamma_i} \cos(\sigma_i) \quad (11)$$

the Hamiltonian is expressed by

$$\begin{aligned}
\mathcal{H} = {}& \tfrac{1}{4}(\delta - 2(C + D))(x_M^2 + y_M^2 + x_U^2 + y_U^2) \\
& + B(x_M^2 + y_M^2 + x_U^2 + y_U^2)^2 \\
& + C(x_M^2 + y_M^2) + D(x_U^2 + y_U^2) \\
& + E(x_M x_U + y_M y_U) \\
& + F(x_M^2 - y_M^2) + G(x_M x_U - y_M y_U) \\
& + H(x_U^2 - y_U^2).
\end{aligned} \quad (12)$$

This Hamiltonian has two degrees of freedom. The state of the system is determined by its coordinates x_i and y_i and the parameter δ.

In Paper I, the authors developed an algebraic mapping to study the Ariel–Umbriel 5:3 commensurability, analogous to the map developed by Wisdom (1982, 1983) to study the motion of asteroids near the 3:1 Kirkwood gap. The Hamiltonian (Eq. (12)) is of the same form as that used in Paper I, and the same mapping can be used to study the Miranda–Umbriel 3:1 resonance, though with a different identification of the variables and different coefficients. The use of the algebraic mapping, which speeds numerical computations by about 3 orders of magnitude over direct integra-

tions and even more than an order of magnitude over the analytically averaged differential equations, allows us to study evolution through the resonance with sufficiently slow simulated tidal dissipation rates. As was discovered by the authors in Paper I, the rate of simulated tidal evolution through the Uranian mean-motion commensurabilities must be extremely slow ($\dot{a}/a < 10^{-10}$ per orbit period) in order for the the numerical simulations to be free of dynamical artifacts. The algebraic mapping provides the most practical way to study the evolution through these resonances.

3. EVOLUTION THROUGH THE RESONANCE

Tidal dissipation within Uranus results in differential decreases in the satellite mean motions. During passage through the resonance, the fractional change in the parameter δ is large compared to the fractional changes in the other coefficients, which will therefore be taken to be constant. The time rate of change of δ is

$$\dot{\delta} = 4\dot{A} \approx (3\dot{n}_U - \dot{n}_M) - 16B(\dot{\Sigma}_M + \dot{\Sigma}_U). \quad (13)$$

Due to tidal dissipation in the planet, the orbits of the satellites expand (e.g., Goldreich 1965),

$$\frac{\dot{a}_i}{a_i} = 3k_2 n_i \frac{m_i}{M} \left(\frac{R}{a_i}\right)^5 \frac{1}{Q}, \quad (14)$$

and the inclinations damp at a rate (Darwin 1880, Kaula 1964, MacDonald 1964) of

$$\frac{\dot{i}_i}{i_i} \approx -\frac{1}{4}\frac{\dot{a}_i}{a_i}, \quad (15)$$

where k_2 and Q are, respectively, the potential Love number and specific dissipation function for Uranus. Using numerical values appropriate for the Uranian satellites (Stone and Miner 1986),

$$\frac{3\dot{n}_U}{\dot{n}_M} \approx \frac{3m_U}{m_M} \left(\frac{a_M}{a_U}\right)^8 \approx 0.12, \quad (16)$$

so the orbit of Miranda expands relative to that of Umbriel. The inclination damping

timescales are very long, at minimum of order 10^{11} years of Miranda and 10^{12} years for Umbriel. The timescales of inclination damping due to the obliquity of the satellite in Cassini state 1 are even longer (see Tittemore 1988). Inclination damping is therefore not important during resonance passage, or even during the subsequent evolution on timescales comparable to the age of the Solar System.

The most significant term in Eq. (13) is therefore

$$\dot{\delta} = -\dot{n}_M \simeq \frac{3G^2M^2m_M^3}{2\Gamma_M^3}\frac{\dot{a}_M}{a_M} . \quad (17)$$

The rate of evolution through the resonance depends on the specific dissipation function Q of Uranus. Q is constrained by the dynamical history of the satellite system (see Peale 1988). The lower limit of 6600 places Miranda and Ariel at the same distance from Uranus at the time of formation of the Solar System. Upper limits on Q can be established if the current orbital configuration can only result from passage through a particular resonance. The upper limit for Q is the value that would allow passage of that resonance near the time of formation of the Solar System.

Numerical exploration of this system is constrained by availability of computer time. Lower dissipation rates (higher Q) require longer integration times. It may not be feasible to integrate a trajectory through a resonance with an effective dissipation rate which is within the constraints described above. We parameterize the effective dissipation rate as script $\mathcal{Q}$, to distinguish the numerical parameter which determines the rate of evolution in our simulation from the physical parameter. We desire a value of $\mathcal{Q}$ low enough that we can adequately study the system, but high enough that artifacts in the dynamics do not appear. In Paper I, it was found that artifacts appeared in the dynamics of the 5:3 resonance even at very slow dissipation rates. We have carried out a similar study

to determine the influence of the rate on the dynamics of the 3:1 resonance.

This study involved integrating identical sets of trajectories through the resonance at different simulated dissipation rates. The initial coordinates for each trajectory in a set were determined as follows. For an initial trajectory, with physical parameters a_M = 4.8642R, a_U = 10.1179R, i_M = 0.005 rad, i_U = 0.005 rad, $\sigma_M = \pi/2$, and $\sigma_U = 3\pi/2$, we compute the coordinates x_M = 0.0, y_M = 0.0009212, x_U = 0.0, and y_U = -0.004574, and the parameter δ = -0.364003. These initial inclinations are comparable to the current inclinations of the Uranian satellites excluding Miranda. From this initial point, the coordinates of 19 additional points, spaced in time by 66 mapping periods ($T = 2\pi/40$ year), were computed. These 20 points formed the initial coordinates of the trajectories, each starting with the same energy, δ, and action (area enclosed by a trajectory in phase space), but with different phases. From these initial coordinates, the trajectories were numerically integrated through the commensurability using the algebraic mapping.

Figure 1 shows the distributions of time-averaged final inclinations for Miranda and Umbriel for a set of 20 trajectories integrated through the 3:1 mean-motion commensurability with a very slow simulated tidal dissipation rate ($\mathcal{Q} = 110$, $\dot{a}_M/a_M = 6 \times 10^{-12}$ per orbit period). There is a distinct bimodal distribution of i_M: some trajectories escape from all of the resonances to lower inclinations, but most trajectories are temporarily captured into resonance, and the orbital inclination of Miranda reaches at least a few degrees before the trajectory escapes from the resonant interaction. It is clear from this figure that there is a significant probability that Miranda could have escaped from the 3:1 resonance with Umbriel with an orbital inclination close to the present value of ~4°. Clearly, the orbit of Umbriel can be significantly affected by the resonant interaction as well. The restricted
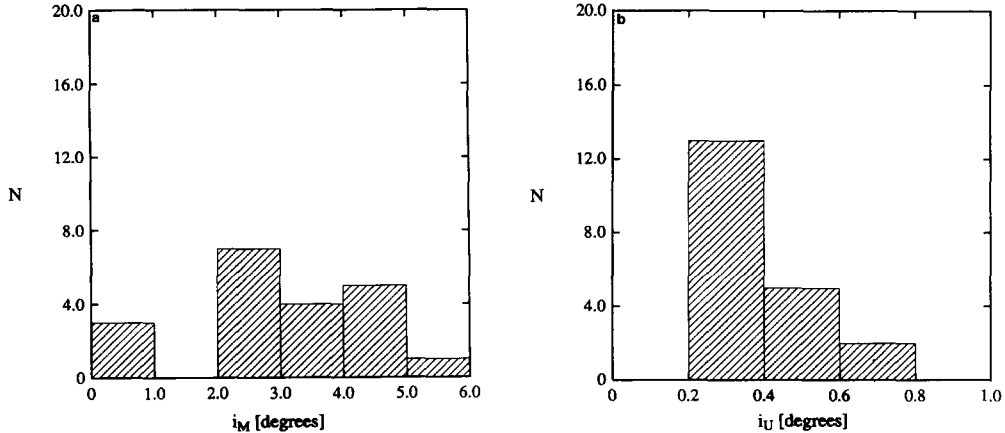
FIG. 1. Distributions of escape orbital inclinations of Miranda (a) and Umbriel (b) for an ensemble of 20 trajectories evolved through the resonance with $\mathcal{Q} = 110$, or $\dot{a}_M/a_M = 6 \times 10^{-12}$ per orbit period. Initially, $i_M = i_U = 0°29$ (see text). Both orbits are affected by the resonant interaction. An orbital inclination of about 4° for Miranda can clearly be attained during passage through the 3 : 1 commensurability with Umbriel.

three-body problem would not be a good approximation for this system.

Figure 1 shows the typical outcomes of trajectories numerically evolved through the resonance with extremely slow simulated tidal dissipation rates. Figure 2 summarizes how this behavior changes as the simulated rate of tidal evolution is increased. In this figure, the mean final inclinations of temporarily captured trajectories are plotted as a function of the simulated rate of evolution, expressed in terms of the effective specific dissipation function of Uranus $\mathcal{Q}$. The error bars are the standard deviations of the mean. For $\mathcal{Q} > 3.3$ ($\dot{a}_M/a_M < 2 \times 10^{-10}$ per orbit period), the mean final orbital inclination of Miranda is close to the current value, much higher than the mean initial value of 0°29. For smaller $\mathcal{Q}$ (higher dissipation rates), the mean final i_M decreases sharply with increasing rate, and for $\mathcal{Q} < 0.33$, the mean final orbital inclinations of Miranda and Umbriel are the same as the initial values: they have been dragged through the resonance without displaying any interesting behavior.
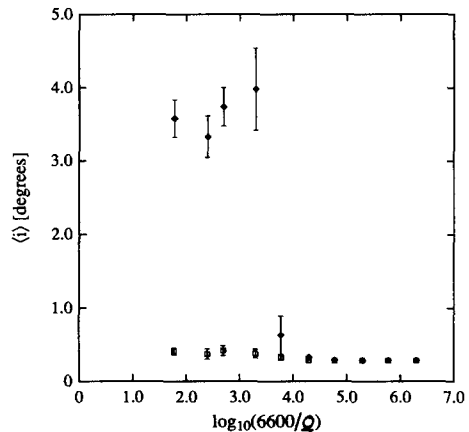
The sudden change in mean final inclina-

FIG. 2. Mean escape orbital inclinations of Miranda (♦) and Umbriel (□) for temporarily captured trajectories as a function of the simulated tidal dissipation rate, expressed in terms of the effective specific dissipation function of Uranus $\mathcal{Q}$. Error bars are standard deviations of the mean; typical distributions of the orbital inclinations for slow simulated tidal evolution rates can be seen in Fig. 1. For $\mathcal{Q} > 3.3$ ($\dot{a}_M/a_M < 2 \times 10^{-10}$ per orbit period), many trajectories are temporarily captured into resonance, and escape with a high value of the orbital inclination of Miranda. For smaller $\mathcal{Q}$, rate-induced artifacts appear in the dynamics; at much higher simulated dissipation rates ($\mathcal{Q} < 0.33$), the trajectories are dragged through the resonance without displaying any interesting behavior.

tion with rate can be understood in the following way. At low inclinations, the resonance behavior is described well by the theory of evolution through isolated mean-motion resonances (see below). This theory assumes that the timescale of evolution of the parameter δ is much longer than the periods of the fundamental frequencies in the problem. These frequencies are the secular frequencies and the frequencies of small-amplitude libration in each of the resonances. The libration frequency of a given resonance increases as a captured trajectory evolves within the resonance, whereas the nonresonant frequencies remain nearly constant over the timescale of resonance passage. We can express the rate of tidal evolution as the change of libration frequency in one libration period divided by the libration frequency ($\Delta\omega_L/\omega_L$). If this dimensionless quantity is of order unity, it is expected that the assumption of adiabatic invariance of the action will no longer be valid, since the timescale of simulated tidal evolution is similar to the dynamical timescales.

The resonance involving only the orbital node of Miranda is the first resonance encountered and we shall refer to it as resonance 1. The Hamiltonian for this resonance considered independently includes only one of the angle-dependent terms in Eq. (9):

$$\mathcal{H}_1 = \tfrac{1}{2}(\delta + 2(C - D) + 16B\Sigma_U)\Sigma_M$$
$$+ 4B\Sigma_M^2 + 2F\Sigma_M \cos(2\sigma_M)). \quad (18)$$

To find the libration frequency, we expand the Hamiltonian about the resonance libration center (pendulum approximation) and consider the motion near the stable fixed point. The frequency of small-amplitude librations for this resonance can thus be expressed as

$$\omega_L^2 = -4F(\delta - \delta_0), \quad (19)$$

where $\delta_0 = -2(C - D) + 4F - 16B\Sigma_U$ is the value at which the libration zones first appear in the phase space of resonance 1 (see

Appendix III of Paper I for details of these calculations). The change in the libration frequency in one period is $\Delta\omega_L \simeq -4\pi F\dot{\delta}/\omega_L^2$. From Eq. (17), with $\dot{a}_M/a_M = 9.4 \times 10^{-14}$ per orbit period for $Q = 6600$, $\dot{\delta} = 4.1 \times 10^{-4}/\mathfrak{Q}$ in our units. For $i_M = i_U = 0.005$ rad well before the resonance is encountered, $\delta_0 = 0.531$. At the point that the trajectory is captured into the resonance, $\delta = 0.563$, and $\Delta\omega_L/\omega_L = 3.6/\mathfrak{Q}$. Therefore, for $\mathfrak{Q} \approx 3.6$, artifacts should begin to appear in the dynamics. In the numerical experiments, significant artifacts appear for $\mathfrak{Q} < 3.3$ ($\dot{a}_M/a_M > 2 \times 10^{-10}$ per orbit period), in excellent agreement with the analytic prediction.

The slowest rate used to integrate many trajectories, $\mathfrak{Q} = 110$ ($\dot{a}_M/a_M = 6 \times 10^{-12}$ per orbit period), with $\Delta\omega_L/\omega_L = 0.03$ (see Fig. 1), is slow enough that this artifact does not influence the dynamics. This has been verified by integrating individual trajectories through the resonance with lower dissipation rates ($\dot{a}_M/a_M = 9 \times 10^{-13}$ per orbit period).

In Fig. 3, the Hamiltonian energies of the trajectories with $\mathfrak{Q} = 110$ (see Fig. 1) are plotted vs δ. We have parameterized the energy in a manner analogous to that used in Paper I: $\Delta E = \mathcal{E} - E_1$, where $\mathcal{E}$ is the value of the Hamiltonian, and

$$E_1 = \begin{cases} 0, & \delta < 2(C - D) + 4H \\ -(\delta - 2(C - D) - 4H)^2/64B, \\ & \delta \geq 2(C - D) + 4H. \end{cases} \quad (20)$$

Positive ΔE indicates the appearance of an excluded region near the origin of that surface of section which plots y_M vs x_M when $x_U = 0$. As in the surfaces of section described in Paper I, the quartic nature of the Hamiltonian means that the section condition $x_U = 0$ can have two or four values of y_U conjugate to x_U, forming four root "families." Associated with the excluded region on the surface of section is a region on the energy surface of the Hamiltonian which connects the "outer" families of roots and

the "inner" root families via the chaotic separatrix. Therefore, with positive ΔE, a trajectory can evolve into the quasiperiodic zone on the inner root families, which allows it to escape from the resonance. As in Paper I, the heavily shaded region in the upper part of the δ, ΔE plot (Fig. 3) is the region in which evolution is not allowed. The region where "macroscopic" chaotic regions may be found, which is most of the accessible region with positive ΔE, is lightly shaded.

The dynamical significance of the parameterization used in Paper I was that positive ΔE indicated forced libration of one of the resonant arguments, due to the division of the energy surface into two regions. In the Miranda–Umbriel 3 : 1 problem, the phase space is not as complicated (see below). The phase space more nearly resembles the pendulum-like phase space of the single-resonance theory. Libration is possible on quasiperiodic islands surrounded by a chaotic separatrix. There is a tiny region of parameter space near the boundary of the prohibited region in Fig. 3 where the energy surface divides the phase space into librating regions, but it does not appear to be significant (it is not even visible at this scale). The new mechanism of capture discovered in the program of research described in Paper I does not appear to be important in the Miranda–Umbriel 3 : 1 resonant interaction.

In the δ, ΔE parameter space, captured trajectories are linear, and escaping trajectories decrease quadratically to large negative ΔE. For the set of trajectories shown in Fig. 3, evolution occurs along three "branches." Quasiperiodic evolution is shown as solid lines, and chaotic behavior is shown as dashed lines. There are two linear (capture) branches and an escape branch. Trajectories on the escape branch escape from all three of the resonances, and evolve to large negative ΔE.

The upper linear branch involves capture into resonance 1. Half of the trajectories in this set were captured into this resonance.
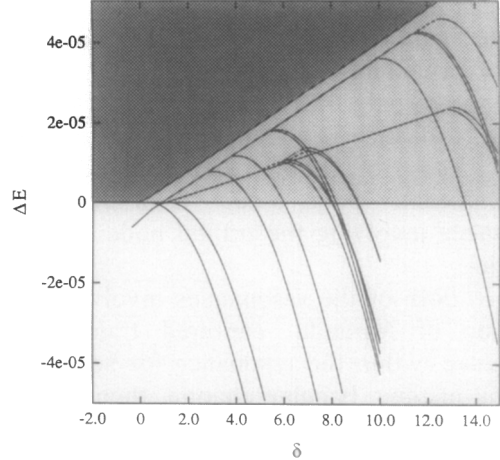

FIG. 3. Trajectories in δ, ΔE parameter space with $\mathfrak{A}$ = 110 (see Fig. 1). Solid lines indicate quasiperiodic behavior and dashed lines indicate chaotic behavior. Evolution occurs along one of three "branches." The upper linear branch involves temporary capture into resonance 1 (i_M^2), and the lower linear branch involves temporary capture into resonance 2 ($i_M i_U$). Trajectories escape to large negative ΔE. The units of δ are year^{-1}.

The single-resonance theory predicts a capture probability of 0.42 for i_M = 0.005 before the resonance is encountered.

The lower linear branch involves capture into the mixed resonance, which we will refer to as resonance 2. Seven of the ten trajectories not captured into resonance 1 were captured into resonance 2. For low values of the inclinations, when the resonance is first encountered, the inclination of Umbriel can be approximated as constant, since the mass of Umbriel is much greater (a factor of about 17) than the mass of Miranda. The mixed resonance then takes the form of a first-order resonance (see Peale 1988), and the probability of capture can be estimated (see, e.g., Henrard and Lemaitre 1983). In this approximation, the single-resonance theory predicts a capture probability of ≈ 0.69 for $i_M \approx 0.003$ after escaping from the first resonance, and i_U = 0.005.

None of the trajectories in this set were captured into the resonance involving only

the orbital node of Umbriel, or resonance 3. The single-resonance theory predicts a very low probability of capture into this resonance of only 0.017 for i_U = 0.005 before the resonance is encountered. The orbital inclination of Umbriel does not decrease significantly upon escape from the resonances involving the orbital node of Umbriel.

In both of the resonances involving the node of Miranda, captured trajectories evolve within the resonance for some period of time, become chaotic, then escape to large negative ΔE. In both cases, escape is only possible within certain ranges of δ, rather than occurring randomly. The dynamical explanation for this is given below.

The energy of the Hamiltonian evolves slowly as δ changes. Since the evolution of the Hamiltonian energy is slow compared to the dynamical timescales, we can "freeze" the Hamiltonian energy and δ at any point in the evolution and study the structure of the phase space by computing surfaces of section, in order to understand

the qualitative behavior of the trajectory. The surface of section that was chosen for study plots y_M vs x_M when x_U = 0. As indicated earlier, the phase space of this problem is not as complicated as the phase space of the Ariel–Umbriel 5 : 3 resonance. The interesting behavior takes place on the outer pair of root families, until the trajectory escapes into that part of phase space including the inner pair. The structures of the phase space on the two root families forming the outer pair are similar. Therefore, the evolution of the trajectory through the resonance can be adequately studied on the root family with the largest numerical value. Furthermore, we have chosen to plot Σ_M vs σ_M rather than y_M vs x_M, in order to better display the pendulum-like structure of the phase space.

Figure 4 shows the evolution of the inclinations with δ for a trajectory captured in resonance 1. The maximum and minimum inclinations of the satellites within a short interval of δ ($\Delta\delta \approx 0.004$) are plotted vs δ. Before the resonance is encountered, the
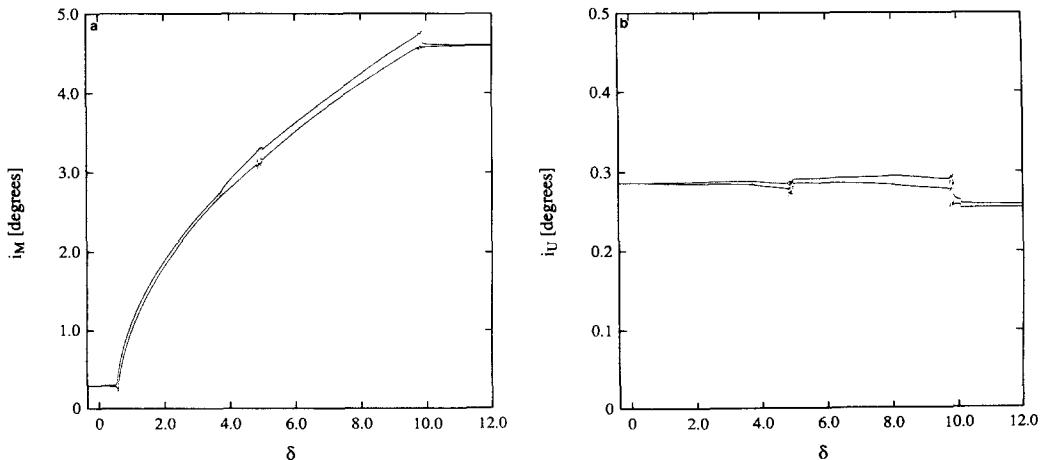

FIG. 4. Variations in the orbital inclinations of Miranda (a) and Umbriel (b) for a trajectory captured into resonance 1 ($\dot{a}_M/a_M$ = 6 × 10^{-12} per orbit period). The maximum and minimum inclinations of each satellite are plotted in intervals of $\Delta\delta \approx 0.004$, where the units of δ are year^{-1}. The evolution is regular and quasiperiodic at low inclination, but secondary resonances between the fundamental frequencies pull the trajectory into the chaotic zone at high inclination. The trajectory can escape from the mean-motion resonance via the chaotic zone, leaving the orbit of Miranda with an inclination comparable to its present value.
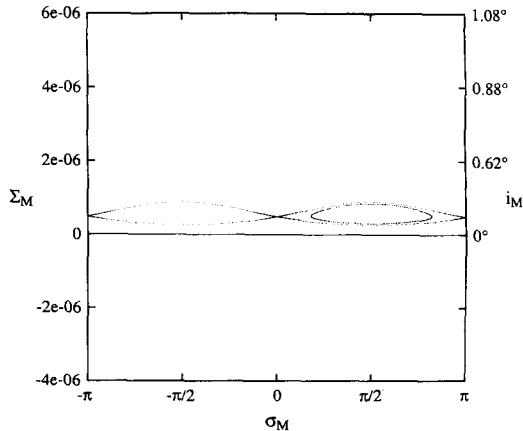
FIG. 5. Surface of section showing the phase space of the trajectory shown in Fig. 4 just after capture into resonance 1 (δ = 0.578). The evolution at this point is well described by the single-resonance theory: there are two libration regions surrounded by a regular-looking separatrix. The trajectory generates the loop in the libration region on the right of the figure.

secular interaction between the satellites is weak, and the inclinations are nearly constant. When the resonance is encountered at low inclination, the trajectory crosses a narrow separatrix into one of two libration zones. In Fig. 5, the trajectory generates the closed loop in the region of libration corresponding to positive σ_M, which it occupies until escaping from the resonance. The separatrix is also displayed in this figure and in subsequent surfaces of section, in order to illustrate the phase space through which the trajectory tidally evolves. After capture into the resonance, the average orbital inclination of Miranda increases proportional to the square root of δ, as predicted by the single-resonance theory. During the quasiperiodic evolution within the resonance, the inclination oscillates smoothly about a gradually increasing mean value. Meanwhile, the averge orbital inclination of Umbriel stays nearly constant, but with gradually increasing oscillations about the mean value. As the inclination increases, perturbations due to the other resonances broaden the separatrix into a chaotic region (Fig. 6). The libration region of the mixed resonance has appeared in the phase space, also surrounded by a chaotic separatrix. In this figure, the trajectory generates the closed loop in the libration region corresponding to positive σ_M.

At $\delta \approx 2.4$ in Fig. 4, there is a small but noticeable decrease in the magnitude of the oscillations about the mean value of the orbital inclination of Miranda. Figure 7 displays a surface of section showing the trajectory at this point in the evolution. The frequency of small-amplitude librations has been increasing as δ increases, and at this point there is a 1 : 4 commensurability between the libration frequency and the frequency of circulation of σ_U. Note that the chaotic regions have continued to increase in width, and the libration regions of the two resonances are nearly overlapping. A secondary resonant structure with four islands has formed within the libration zone of resonance 1, due to the fact that there is a 1 : 4 commensurability between the frequency of libration of σ_M and the frequency of circulation of σ_U. As δ evolves, the chain of islands moves away from the libration center, eventually encountering the trajec-
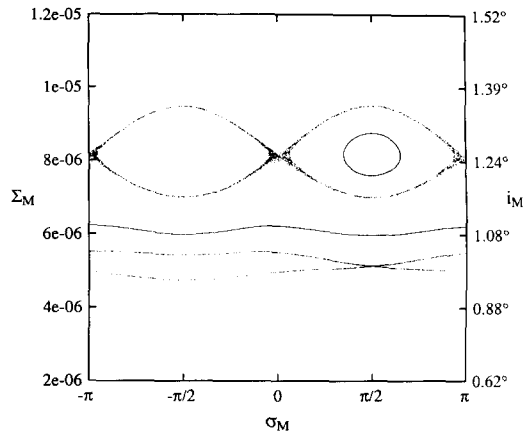

FIG. 6. Surface of the section for the trajectory shown in Fig. 4 at δ = 1.206. The trajectory generates the loop in the libration region on the right of the figure. The libration zone of the mixed ($i_M i_U$) resonance has appeared on the section. The chaotic separatrix has become significantly wider. The width of the chaotic separatrix agrees well with analytic estimates.
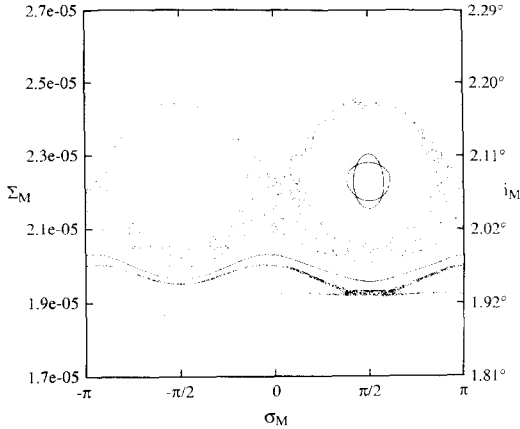
FIG. 7. Surface of section for the trajectory shown in Fig. 4 at $\delta = 2.358$. The chaotic zones have continued to increase in width. The trajectory has just encountered a secondary 1 : 4 resonance between the libration frequency in the i_M^2 resonance and the frequency of circulation of σ_U, and it therefore traces out the period-4 separatrix associated with this secondary resonance in the libration zone on the right of the figure. This particular trajectory is not captured into the secondary resonance.

tory. In Fig. 7, the trajectory traces out the separatrix associated with this secondary resonance in the libration region on the right of the figure. The trajectory must cross the separatrix, and may either become trapped in the island structure or escape to the region near the libration center. The trajectory in Fig. 4 passes through the secondary commensurability without becoming trapped on the islands, but as it does so, the area enclosed by the trajectory on the phase plane decreases from a value corresponding to the area enclosed by the outer boundary of the separatrix at the point of transition to a value corresponding to the area enclosed by the inner boundary of the separatrix at the point of transition. When the area enclosed by the trajectory decreases, so does the amplitude of oscillation of the inclination about the mean value in the libration region, as seen in Fig. 4 at $\delta \approx 2.4$

At a somewhat higher value of δ ($\delta \approx 3.7$), the trajectory encounters a 1 : 3 commensurability between the same two fre-

quencies (Fig. 8). This time, the trajectory is trapped in the island structure, and as δ increases, the islands are pulled away from the libration center (Fig. 9). As this takes place, the amplitude of the oscillations of the inclination of Miranda increases (see Fig. 4) as the trajectory visits each island on the surface of section sequentially. At the same time, the mean orbital inclination of Umbriel decreases slightly.

Figure 10 shows the phase space just before the trajectory enters the chaotic zone. The three loops generated by the trajectory seen in Fig. 9 have themselves been broken into chains of islands: the trajectory has been captured into a yet higher order resonance. In Fig. 11, we see the neighborhood of one set of these islands in Fig. 10 at an expanded scale, with other trajectories plotted as well to illustrate the structure of the surrounding phase space. The trajectory shown in Fig. 4, which is still quasiperiodic at this point, generates the seven star-shaped islands, which are now fully
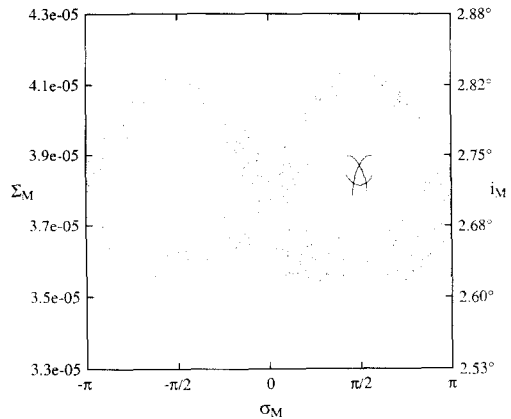

FIG. 8. Surface of section for the trajectory shown in Fig. 4 at $\delta = 3.614$. The chaotic zones surrounding the two libration regions have merged, in agreement with the predictions of the resonance overlap criterion. The trajectory has just encountered a 1 : 3 secondary resonance between the libration frequency in the i_M^2 resonance and the frequency of circulation of σ_U, and traces out the period-3 separatrix in the libration zone on the right of the figure. The trajectory is captured into this secondary resonance.
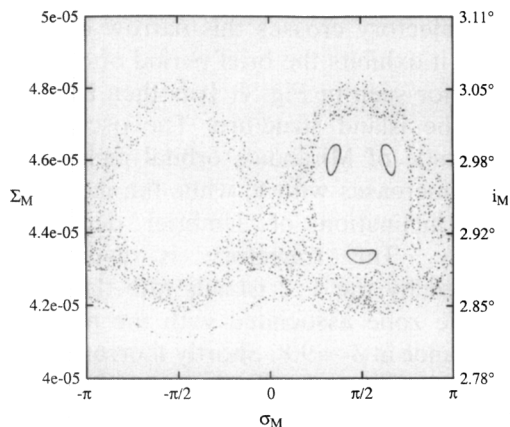
FIG. 9. Surface of section for the trajectory shown in Fig. 4 at $\delta = 4.242$. The trajectory, which generates the three quasiperiodic islands in the libration region on the right of the figure, is being dragged away from the libration center due to capture into the 1:3 secondary resonance.

surrounded by the chaotic zone. The shapes of these islands are characteristic of a period-4 instability bifurcation (see, e.g., Hénon 1969). This cascade of higher and higher order resonances is characteristic of

the development of chaotic instabilities in nonlinear dynamical systems.

At $\delta \approx 4.8$, the trajectory becomes chaotic. During evolution through the chaotic region, the variations of inclination are irregular, but the average inclination of Miranda continues to increase. The chaotic zones surrounding the libration zones of the i_M^2 and $i_M i_U$ resonances now overlap, and the chaotic zone is a dominant feature of the phase space. Although escape from the orbital resonance is possible during this period of chaotic evolution, the trajectory shown in Fig. 4 enters the libration zone of resonance 1 again at $\delta \approx 5.0$ and becomes quasiperiodic, with a much larger amplitude of oscillation than it had before encountering the 1:3 secondary commensurability.

At $\delta \approx 8.0$ there is a short period of chaotic behavior when the trajectory encounters the 1:2 commensurability between the same two frequencies (Fig. 12). The chaotic separatrix associated with this secondary commensurability has a visible width. As
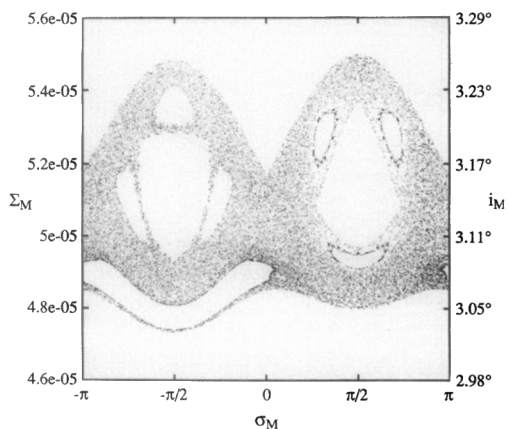

FIG. 10. Surface of section for the trajectory shown in Fig. 4 at $\delta = 4.766$. The trajectory generates the 21 tiny islands in three groups near the boundaries of the stable regions associated with the 1:3 secondary resonance, near the edge of the libration zone on the right of the figure. The trajectory has been dragged out of the secondary resonance by a yet higher order resonance.
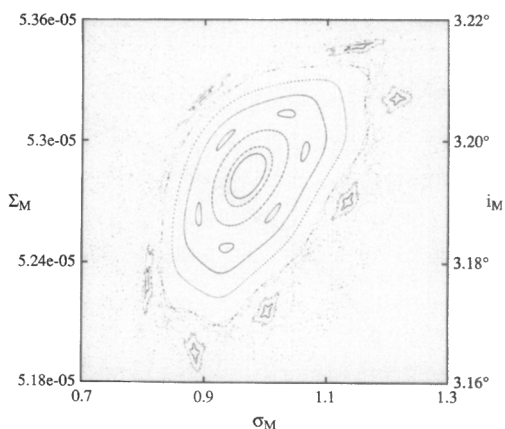

FIG. 11. This is a portion of the phase space shown in the previous figure, but at a larger scale and with more trajectories plotted. The still-quasiperiodic trajectory generates the seven star-shaped islands in the chaotic zone, which are themselves undergoing a period-4 instability bifurcation. This cascade of higher-order resonances is characteristic of the development of chaotic instabilities in nonlinear dynamical systems.
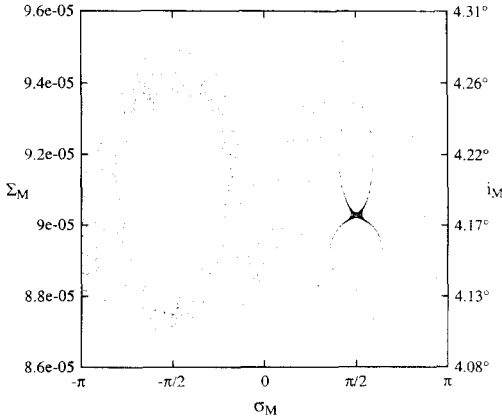
FIG. 12. Surface of section for the trajectory shown in Fig. 4 at $\delta = 8.011$. The trajectory, having returned to the libration region from the large chaotic zone, has just encountered the $1:2$ secondary resonance between the libration frequency in the i_M^2 resonance and the frequency of circulation of σ_U. The trajectory traces out the separatrix associated with this secondary commensurability, which is visibly chaotic. As the trajectory becomes chaotic briefly while crossing this narrow chaotic zone, it causes the feature at $\delta \approx 8.0$ in Fig. 4. The trajectory is captured into this secondary resonance and is again dragged into the large chaotic zone, from which it escapes the mean-motion resonance.

the trajectory crosses this narrow chaotic zone, it exhibits the brief period of chaotic behavior seen in Fig. 4. It is then trapped into the island structure. The oscillation amplitude of Miranda's orbital inclination again increases with δ, while the mean orbital inclination of Umbriel decreases slightly. The trajectory is eventually dragged by the $1:2$ islands into the large chaotic zone associated with the primary resonance at $\delta \approx 9.8$. Shortly thereafter the trajectory shown in Fig. 4 escapes from the resonance, with orbital inclinations of about 4°6 for Miranda and 0°26 for Umbriel.

Figure 13 shows the behavior of the inclinations for a trajectory captured into resonance 2. Again, well before the resonance is encountered, the mutual perturbations are weak, and the inclinations are nearly constant. This time, the trajectory escapes from the first resonance, and the mean orbital inclination of Miranda decreases suddenly as it crosses the separatrix. The trajectory is then captured into the mixed $(i_M i_U)$ resonance, and both inclinations oscillate about mean values that increase
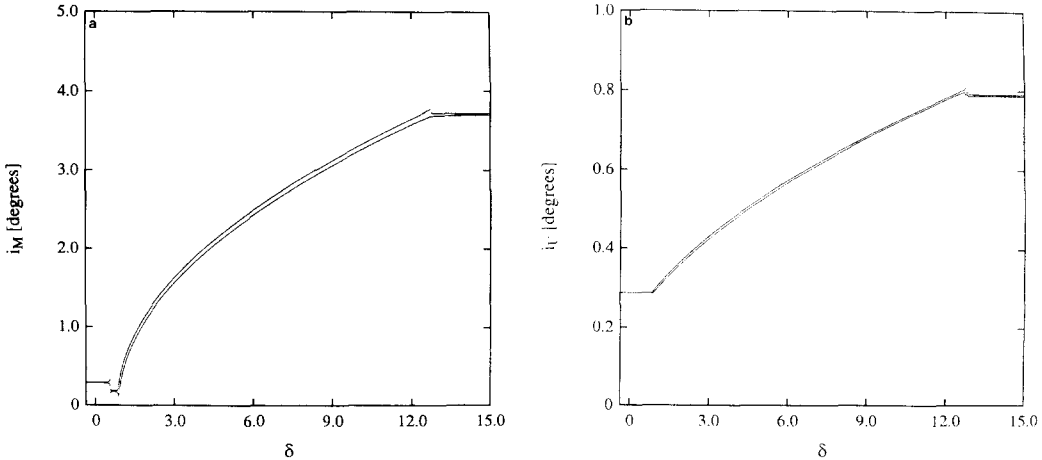

FIG. 13. Variations in the orbital inclinations of Miranda (a) and Umbriel (b) for a trajectory captured into resonance 2 ($\dot{a}_M/a_M = 6 \times 10^{-12}$ per orbit period). The maximum and minimum inclinations of each satellite are plotted in intervals of $\Delta\delta \approx 0.005$, where the units of δ are year^{-1}. The inclinations of both orbits increase during the temporary quasiperiodic phase of evolution within the resonance. Secondary resonances between the degrees of freedom pull the trajectory into the chaotic zone at high inclination. The trajectory can escape from the mean-motion resonance via the chaotic zone, leaving the orbit of Miranda with an inclination comparable to its present value.
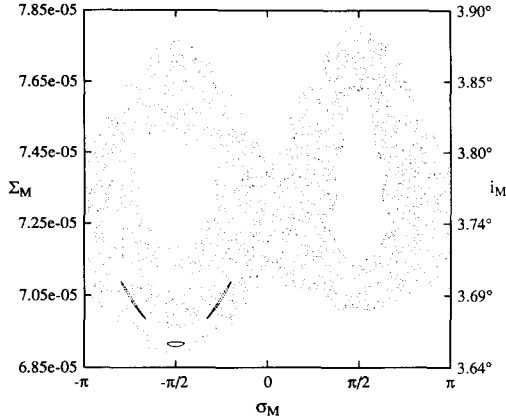
FIG. 14. Surface of section showing the phase space of the trajectory shown in Fig. 13 at $\delta = 12.512$, just before escaping from the resonance. The trajectory generates the three quasiperiodic islands in the libration region of the mixed resonance, and is being dragged away from the libration center. It is possible for a trajectory to jump from one libration region to another via the chaotic zone.

with time (δ). At $\delta \approx 6.0$ and $\delta \approx 7.8$ there are sudden changes in the oscillation amplitudes similar to those described above in Fig. 4. Figure 14 shows the surface of section for this trajectory at $\delta \approx 12.5$, just before it enters the chaotic region. Note that

the trajectory generates three islands, which are being pulled away from the libration center of the $i_M i_U$ resonance as δ increases. These islands occupy a region of phase space in which the argument of the mixed resonance $(\sigma_M + \sigma_U)/2$ librates, although this is not obvious in the variables plotted. At $\delta \approx 12.7$, the trajectory is dragged into the chaotic zone, which also surrounds the neighboring libration zone for resonance 1. It is possible for a trajectory, after entering the chaotic region, to temporarily enter the librating region of resonance 1. The trajectory in Fig. 13 escapes shortly after entering the chaotic zone, leaving Miranda with an average orbital inclination of about $3°7$ and Umbriel with an average orbital inclination of about $0°79$.

Figure 15 shows the inclinations of Miranda and Umbriel during evolution through the 3 : 1 commensurability, with a higher initial inclination for Miranda ($i_M = 1.0°$). Even with this high initial value, the trajectory is captured into the mixed ($i_M i_U$) resonance, and escapes with an i_M comparable to the current value.

The mechanism of escape in all cases of temporary capture appears to require the presence of the secondary resonances be-
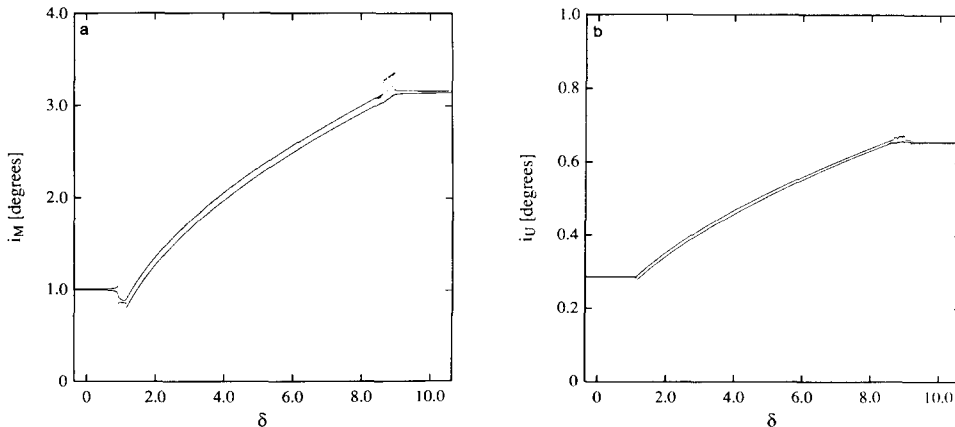
FIG. 15. Variations in the orbital inclinations of Miranda (a) and Umbriel (b) for a trajectory with initial $i_M = 1°0$ ($\dot{a}_M/a_M = 6 \times 10^{-12}$ per orbit period). The maximum and minimum inclinations of each satellite are plotted in intervals of $\Delta\delta \approx 0.0036$, where the units of δ are year^{-1}. Even with the large initial value of i_M, this trajectory is captured into the mixed ($i_M i_U$) resonance, and the orbital inclination of Miranda evolves to a relatively high value.

tween the libration frequency and other fundamental frequencies. The points in the evolution at which these secondary commensurabilities are encountered can be estimated by comparing the frequencies of small-amplitude libration for the resonances considered independently to the fundamental frequencies of the nonresonant part of the Hamiltonian.

The largest contributions to the nonresonant Hamiltonian are given by the expression

$$\mathcal{H}_0 = \tfrac{1}{2}(\delta + 2(C - D))\Sigma_M + \tfrac{1}{2}(\delta - 2(C - D))\Sigma_U + 4B(\Sigma_M + \Sigma_U)^2. \quad (21)$$

Therefore, the "zeroth-order frequencies of the system are

$$\dot{\sigma}_M = \frac{\partial \mathcal{H}_0}{\partial \Sigma_M} = \tfrac{1}{2}(\delta + 2(C - D))$$
$$+ 8B(\Sigma_M + \Sigma_U)$$

$$\dot{\sigma}_U = \frac{\partial \mathcal{H}_0}{\partial \Sigma_U} = \tfrac{1}{2}(\delta - 2(C - D))$$
$$+ 8B(\Sigma_M + \Sigma_U)$$

$$= \dot{\sigma}_M - 2(C - D). \quad (22)$$

For resonance 1, the average value of $\dot{\sigma}_M$ is zero. Therefore, $\dot{\sigma}_U \approx -2(C - D)$, which has the same magnitude as the difference between the frequencies of resonance 1 and resonance 2, or, equivalently, the difference between the frequencies of regression of Ω_M and Ω_U. The commensurabilities between the degrees of freedom should occur where the libration frequency of resonance 1 (Eq. (19)) and $\dot{\sigma}_U$ form integer ratios. The most important of these commensurabilities, and the values of δ and i_M at which they occur, are summarized in Table I.

TABLE I

FREQUENCY RATIOS:
RESONANCE 1

$\omega_L : \dot{\sigma}_U$	δ	i_M
1 : 4	2.3	2.0°
1 : 3	3.6	2.7°
1 : 2	7.5	4.1°

TABLE II

FREQUENCY RATIOS: RESONANCE 2

$\omega_L : (\dot{\sigma}_M - \dot{\sigma}_U)$	δ	i_M	i_U
1 : 5	5.8	2.4°	0.5°
1 : 4	8.6	3.0°	0.6°
1 : 3	14.6	4.0°	0.8°

There is a good correlation between the analytical predictions and the numerical results.

As indicated earlier, the mixed resonance can be approximated as a first-order resonance when it is first encountered by the trajectory, and the inclination of Umbriel is nearly constant ($\Sigma_M \ll \Sigma_U$). After the trajectory is captured, the phase space of the mixed resonance is quite complicated (see also Sinclair 1974) as both inclinations increase. For large δ, the mixed resonance can be approximated as a second-order resonance in $(\sigma_M + \sigma_U)/2$, and $\Sigma_M \approx \Sigma_U$. In this approximation, the Hamiltonian for resonance 2 becomes

$$\mathcal{H}_2 = (\delta + 16B\Sigma_{U0})\Sigma_M + 16B\Sigma_M^2 + 2G\Sigma_M \cos(\sigma_M + \sigma_U). \quad (23)$$

The frequency of libration of the mixed resonance argument $(\sigma_M + \sigma_U)/2$ is therefore

$$\omega_L^2 \approx 2G(\delta + 2G + 16B\Sigma_{U0}). \quad (24)$$

The average value of $\dot{\sigma}_M + \dot{\sigma}_U$ is zero in the mixed resonance, so the frequency of circulation of the other degree of freedom $\dot{\sigma}_M - \dot{\sigma}_U = 2(C - D)$. The most important commensurabilities between these two degrees of freedom are summarized in Table II. Again, the correlation between these predicted values and the results of the numerical simulations (e.g., Figs. 13 and 15) is very good. Note that the values of δ and i_M at which the trajectory enters the chaotic zone are larger than the values at which the secondary resonances are encountered, due to the time it takes for the islands to be dragged away from the libration center and into the chaotic zone.

The full Hamiltonian of this problem is coupled through both linear and nonlinear terms. The strength of the coupling increases as the inclination(s) increase during temporary capture into one of the resonances. Therefore, the "zeroth-order" frequencies described above are modified, and the motion becomes more complicated. Secondary resonances between the libration frequency and various frequency components of this more complicated motion are possible, but do not appear to significantly affect the evolution.

Because the chaotic zone does not completely engulf the libration regions, it is possible for a trajectory to be permanently captured into a resonance, if it passes through all of the secondary commensurabilities between the degrees of freedom.

The limited extent of the chaotic region can be understood by considering the theoretical estimate of the width of a perturbed separatrix (Chirikov 1979). The half-width of the separatrix is expressed in terms of the chaotic variation of the energy integral for the perturbed resonance,

$$\frac{\Delta \mathscr{E}}{\mathscr{E}_{sx}} = 4\pi \varepsilon \lambda^3 e^{-\pi\lambda/2}, \qquad (25)$$

where λ is the ratio of the perturbation frequency to the frequency of small-amplitude librations and the perturbation parameter ε is the ratio of the coefficients of the perturbing term to the coefficients of the perturbed term.

For perturbations of resonance 1 by resonance 2, the perturbed Hamiltonian can be written

$$\mathscr{H} = \mathscr{H}_1 + \varepsilon \mathscr{V}, \qquad (26)$$

where $\mathscr{H}_1$ is given in Eq. (18) and

$$\varepsilon \mathscr{V} = 2G\sqrt{\Sigma_M \Sigma_U} \cos(\sigma_M + \sigma_U). \qquad (27)$$

Therefore

$$\lambda = \frac{\dot{\sigma}_M - \dot{\sigma}_U}{\omega_L} = \frac{C - D}{\sqrt{-F(\delta - \delta_0)}} \qquad (28)$$

and

$$\varepsilon = -\frac{G}{F}\sqrt{\frac{\Sigma_U}{\Sigma_{M_1 R}}} = -\frac{G}{F}\sqrt{\frac{-8B\Gamma_U}{\delta - \delta_0}} \, i_U, \qquad (29)$$

where

$$\Sigma_{M_1 R} = \frac{(\delta - \delta_0)}{-16B} \qquad (30)$$

is the libration center of resonance 1. Due to the secular interaction, ε and λ are time-dependent in the full problem. However, since the secular interaction is weak, the variations are small.

For small values of δ the separatrix width is exceedingly small, but it increases exponentially as the libration frequency increases. However, for large values of δ, the exponential contribution in Eq. (25) approaches 1 asymptotically, while the factors out front decrease quadratically with δ, so $\Delta\mathscr{E}/\mathscr{E}_{sx}$ decreases. Note that the perturbation parameter ε is linear in i_U.

However, because of the overlap of the libration regions of resonance 1 and resonance 2 at large values of δ, the chaotic zone will be larger than predicted by Eq. (25). The resonance overlap criterion (Chirikov 1979) predicts large-scale chaos where the sum of the half-widths of the libration regions plus the half-widths of the chaotic separatrices exceeds the spacing between libration centers. The point at which the libration regions overlap can be estimated, using the formulae for the resonances considered independently. The extent of the libration region for resonance 1 is given by

$$\Sigma_{M_1} = \Sigma_{M_1 R} \pm \Delta\Sigma_{M_1}, \qquad (31)$$

where

$$\Delta\Sigma_{M_1} = \begin{cases} \Sigma_{M_1 R}, & \delta_0 \leq \delta < -2(C - D) - 4F + 16B\Sigma_U \\ \dfrac{\sqrt{-F(-4B\Sigma_{M_1 R} + F)}}{-2B}, & \delta \geq -2(C - D) - 4F + 16B\Sigma_U. \end{cases} \qquad (32)$$

For large δ, the extent of the libration region for resonance 2 can be expressed as (see Eq. (23))

$$\Sigma_{M_2} = \Sigma_{M_2R} \pm \Delta\Sigma_{M_2}$$
$$\approx \Sigma_{M_2R} \pm \frac{\sqrt{G(-16B\Sigma_{M_2R} - G)}}{-8B}.$$

(33)

For a trajectory captured into resonance 1, σ_M is oscillating, while the argument of resonance 2, $(\sigma_M + \sigma_U)/2$, circulates with a frequency $-(C - D) \approx -0.165$ year^{-1}. Therefore, at the center of the resonance 2 island, $\dot{\sigma}_M = C - D \approx 0.165$ year^{-1}. Since $\dot{\sigma}_M = \partial\mathcal{H}_1/\partial\Sigma_M$ for resonance 1, this frequency difference can be related to a difference in Σ_M between libration centers. The stable equilibrium on the surface of section corresponding to the largest quartic root ($\sigma_U = \pi/2$) is at $\sigma_M = -\pi/2$, so $\sigma_M + \sigma_U = 0$. Therefore, for a trajectory captured into the libration zone of resonance 1, the center of libration of resonance 2 is at

$$\Sigma_{M_2R} = \frac{(\delta - (\delta_0 + 2(C - D)))}{-16B}$$

(34)

for $\delta \geq \delta_0 + 2(C - D)$. Σ_{M_2R} maintains a nearly constant separation from Σ_{M_1R} on the
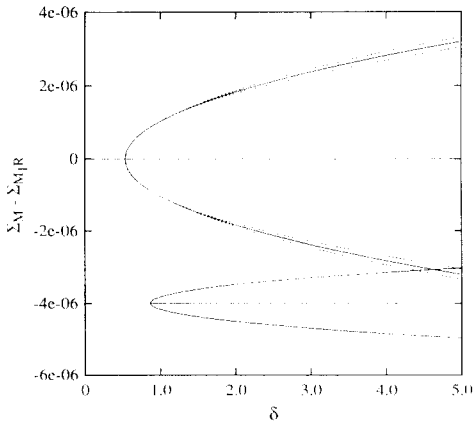

FIG. 16. Analytic predictions of the positions and widths of the libration zones of the i_M^2 and $i_M i_U$ resonances (solid lines) relative to the libration center of the i_M^2 resonance, and the width of the chaotic separatrix of the i_M^2 resonance (dashed lines). Large-scale chaos is present when the libration regions merge.
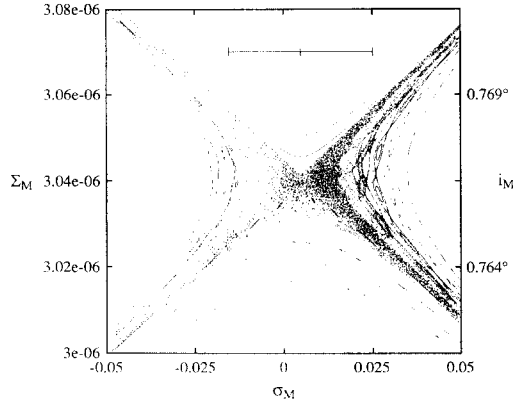

FIG. 17. Surface of section showing the phase space of the trajectory shown in Fig. 4 shortly after capture into resonance 1 ($\delta = 0.788$), with $\Delta\mathcal{E}/\mathcal{E}_{sx} = 8.3 \times 10^{-4}$. The region near one of the unstable fixed points is shown. The bar denotes the analytic prediction of the width of the chaotic separatrix near the unstable fixed point. Although the boundary of the chaotic region is not well defined, the distances of the points furthest from the center of the chaotic zone at its narrowest extent agree well with the predicted width. The fact that the invariant curves just outside the large chaotic zone are slightly further from the center than the predicted width supports this result.

phase plane defined by σ_M and Σ_M until the chaotic separatrices merge.

For the case where resonance 1 is perturbed by resonance 2, the unperturbed libration widths, as well as $\Delta\mathcal{E}/\mathcal{E}_{sx}$ for resonance 1 ($i_U = 0.005$), are plotted in Fig. 16. The libration width plotted for resonance 2 is from the second-order resonance approximation described above, which is a good approximation only for the larger values of δ represented. The predicted value of δ at which the libration zones should overlap is about 4.3. For the trajectory shown in Fig. 4, the two libration zones overlap for $\delta \approx 3.6$. In the real system, of course, the shape of each libration zone is distorted by the presence of the other. The width of each chaotic separatrix tends to be larger on the side nearest the other libration region.

Figure 17 illustrates the accuracy with which the Chirikov formula (Eq. (25)) can be used to predict the width of the chaotic

separatrix. The phase space in the neighborhood of one of the unstable fixed points predicted by the single-resonance theory is displayed. The trajectory (not shown on the figure at this scale) has been captured into the resonance, but is at a point in the evolution well before the value of δ at which resonance overlap is predicted. The bar in the figure denotes the analytic estimate of the width $\Delta\sigma$ of the large chaotic zone near the unstable fixed point. There is good agreement between the predicted width and the maximum $\Delta\sigma$ at which points appear in the large chaotic zone at its narrowest extent. Note, however, that the edge of the chaotic region is ill-defined: it breaks up into narrow connected bands surrounding chains of quasiperiodic islands, and forms a very complicated filamentary structure. Outside of the large chaotic zone, the narrow chaotic separatrices surrounding chains of islands are isolated by invariant curves. The predicted width is close to but within the $\Delta\sigma$ at which the invariant curves appear on the figure at the edge of the large chaotic zone. The accuracy of the analytic formula in predicting the width of the chaotic zone has been similarly verified over 5 orders of magnitude of $\Delta\mathscr{E}/\mathscr{E}_{sx}$.

The success of the single-resonance theory in describing this system at low inclinations can be understood by considering the width of the chaotic zone at the point of capture into the resonance. Equation (25) predicts that the relative width of the separatrix at the point of capture is approximately $\Delta\mathscr{E}/\mathscr{E}_{sx} \approx 5.0 \times 10^{-15}$. For $Q = 6600$, the change in the Hamiltonian energy of the trajectory relative to the separatrix in one libration period is about *12 orders of magnitude* larger than the separatrix width. The trajectory is very quickly pulled across this narrow separatrix by the tidal action. Therefore, chaotic behavior does not affect the process of initial capture into the resonance, if the inclinations of the satellites were comparable to the values we have chosen prior to encountering the resonance.

4. RESONANT PERTURBATIONS

In this section we consider the effect of the eccentricity-type resonances associated with the Miranda–Umbriel 3 : 1 mean-motion commensurability on the evolution of the inclinations.

In the development of the Hamiltonian for the eccentric-inclined problem, the following eccentricity-dependent terms are added to the terms given in Eqs. (1)–(4):

$$
\begin{aligned}
\mathscr{H}_e = \; & -\frac{GMm_M}{2a_M} J_2 \left(\frac{R}{a_M}\right)^2 \left[1 + \frac{3}{2} e_M^2\right] \\
& -\frac{GMm_U}{2a_U} J_2 \left(\frac{R}{a_U}\right)^2 \left[1 + \frac{3}{2} e_U^2\right] \\
& -\frac{Gm_M m_U}{a_U} \left[(1)^{(0)} + (2)^{(0)} \left(\frac{e_M}{2}\right)^2\right. \\
& \quad + (3)^{(0)} \left(\frac{e_U}{2}\right)^2 \\
& \quad \left. + (21)^{(-1)} \frac{e_M}{2} \frac{e_U}{2} \cos(\bar\omega_M - \bar\omega_U)\right] \\
& -\frac{Gm_M m_U}{a_U} \left[(172)^{(3)} \left(\frac{e_M}{2}\right)^2 \right. \\
& \quad \cos(3\lambda_U - \lambda_M - 2\bar\omega_M) \\
& \quad + (182)^{(2)} \frac{e_M}{2} \frac{e_U}{2} \\
& \quad \cos(3\lambda_U - \lambda_M - \bar\omega_M - \bar\omega_U) \\
& \quad + (192)^{(1)} \left(\frac{e_U}{2}\right)^2 \\
& \quad \left. \cos(3\lambda_U - \lambda_M - 2\bar\omega_U)\right].
\end{aligned}
\tag{35}
$$

The first set of terms is due to the planetary oblateness, the second set is due to the secular interaction, and the final set is due to the eccentricity-dependent resonant interaction. Note that (see Leverrier 1855)

$$(1)^{(0)} = \frac{1}{2} b_{1/2}^0(\alpha)$$

$$(2)^{(0)} = \alpha \frac{d}{d\alpha} b_{1/2}^0(\alpha) + \frac{1}{2} \alpha^2 \frac{d^2}{d\alpha^2} b_{1/2}^0(\alpha)$$

$$(3)^{(0)} = (2)^{(0)}$$

$$(21)^{(-1)} = 2b_{1/2}(\alpha) - 2\alpha \frac{d}{d\alpha} b_{1/2}(\alpha)$$

$$- \alpha^2 \frac{d^2}{d\alpha^2} b_{1/2}(\alpha)$$

$$(172)^{(3)} = \frac{21}{2} b_{1/2}^3(\alpha) + 5\alpha \frac{d}{d\alpha} b_{1/2}^3(\alpha)$$

$$+ \frac{1}{2} \alpha^2 \frac{d^2}{d\alpha^2} b_{1/2}^3(\alpha)$$

$$(182)^{(2)} = -20b_{1/2}^2(\alpha) - 10\alpha \frac{d}{d\alpha} b_{1/2}^2(\alpha)$$

$$- \alpha^2 \frac{d^2}{d\alpha^2} b_{1/2}^2(\alpha)$$

$$(192)^{(1)} = \frac{17}{2} b_{1/2}^1(\alpha) + 5a \frac{d}{d\alpha} b_{1/2}^1(\alpha)$$

$$+ \frac{1}{2} \alpha^2 \frac{d^2}{d\alpha^2} b_{1/2}^1(\alpha) - \frac{27}{2} \alpha - \frac{3}{2} \frac{1}{\alpha^2} \tag{36}$$

and α is the ratio of semimajor axes, and b_s^j (α) are Laplace coefficients. The last two terms in the expression for $(192)^{(1)}$ are due to indirect terms in the disturbing function, and arise because the planet-centered coordinate system is not an inertial one.

We define $\psi_i = \frac{1}{2}(3n_U - n_M - 2\bar{\omega}_i)$, $\Psi_i \approx (\Gamma_i/2)e_i^2$, $\Gamma_M = L_M + \frac{1}{2}(\Sigma_M + \Sigma_U + \Psi_M + \Psi_U)$, and $\Gamma_U = L_U - \frac{3}{2}(\Sigma_M + \Sigma_U + \Psi_M + \Psi_U)$.

Expanded in terms of these canonical coordinates, the eccentric-inclined Hamiltonian may be expressed as

$$\begin{aligned}
\mathcal{H} = &\ 2A(\Sigma_M + \Sigma_U + \Psi_M + \Psi_U) \\
&+ 4B(\Sigma_M + \Sigma_U + \Psi_M + \Psi_U)^2 \\
&+ 2C\Sigma_M + 2D\Sigma_U \\
&+ 2E\sqrt{\Sigma_M\Sigma_U} \cos(\sigma_M - \sigma_U) \\
&+ 2F\Sigma_M \cos(2\sigma_M) \\
&+ 2G\sqrt{\Sigma_M\Sigma_U} \cos(\sigma_M + \sigma_U) \\
&+ 2H\Sigma_U \cos(2\sigma_U) \\
&+ 2I\Psi_M + 2J\Psi_U \\
&+ 2K\sqrt{\Psi_M\Psi_U} \cos(\psi_M - \psi_U) \\
&+ 2L\Psi_M \cos(2\psi_M) \\
&+ 2M\sqrt{\Psi_M\Psi_U} \cos(\psi_M + \psi_U) \\
&+ 2N\Psi_U \cos(2\psi_U). \tag{37}
\end{aligned}$$

The expressions for the coefficients $A - N$ are given in Appendix I.

This is now a four degree of freedom Hamiltonian problem with slow time dependence. There are three eccentricity resonances, three inclination resonances, and secular interactions. The eccentricities are coupled to the inclinations through the nonlinear terms. δ is redefined to be the nonresonant contributions to $3n_U - n_M - \dot{\bar{\omega}}_M - \dot{\bar{\omega}}_U - \dot{\Omega}_M - \dot{\Omega}_U$. The coefficients are defined at $\delta = 0$ for $i_i = 0$, $e_i = 0$, and $a_U = 10.1179$, which corresponds to $a_M = 4.8662$. The numerical values of the coefficients for this system are (see Appendix I): $B = -5164.15$, $C = 0.043833$, $D = -0.120829$, $E = -0.0006763$, $F = -0.0009778$, $G = 0.0003939$, $H = -0.00003967$, $I = -0.312892$, $J = 0.1482294$, $K = 0.0003939$, $L = -0.007068$, $M = 0.0052597$, and $N = 0.0006012$. $\Gamma_M = 0.03395267$ and $\Gamma_U = 0.836831$. An algebraic mapping has been developed for this system, analogous to the two degree of freedom mapping.

The inclination resonances are encountered first. Since $3n_U - n_M$ is negative before the commensurability is reached, and the secular contributions to the $\dot{\Omega}_i$ are retrograde, while those of $\dot{\bar{\omega}}_i$ are prograde, the condition $3n_U - n_M - 2\dot{\Omega}_i = 0$ will be met before the condition $3n_U - n_M - 2\dot{\bar{\omega}}_i = 0$.

Figure 18 shows the inclinations (a and b) and eccentricities (c and d) for a trajectory computed for this system. Before the resonances are encountered, the secular interactions of the eccentricities and the inclinations are weak. When the trajectory encounters the inclination resonances, it is captured into resonance 1. The evolution through resonance 1 does not appear to be significantly affected by the presence of the nonresonant eccentricity variations. At first, the evolution is quasiperiodic, showing the same features as were seen in the circular-inclined case. At $\delta \approx 2.4$, the amplitude of oscillation of the orbital inclination of Miranda decreases slightly during passage through the $1:4$ commensurability between the degrees of freedom. At $\delta \approx 3.6$, the trajectory is captured into the secondary $1:3$ commensurability. As the tra-
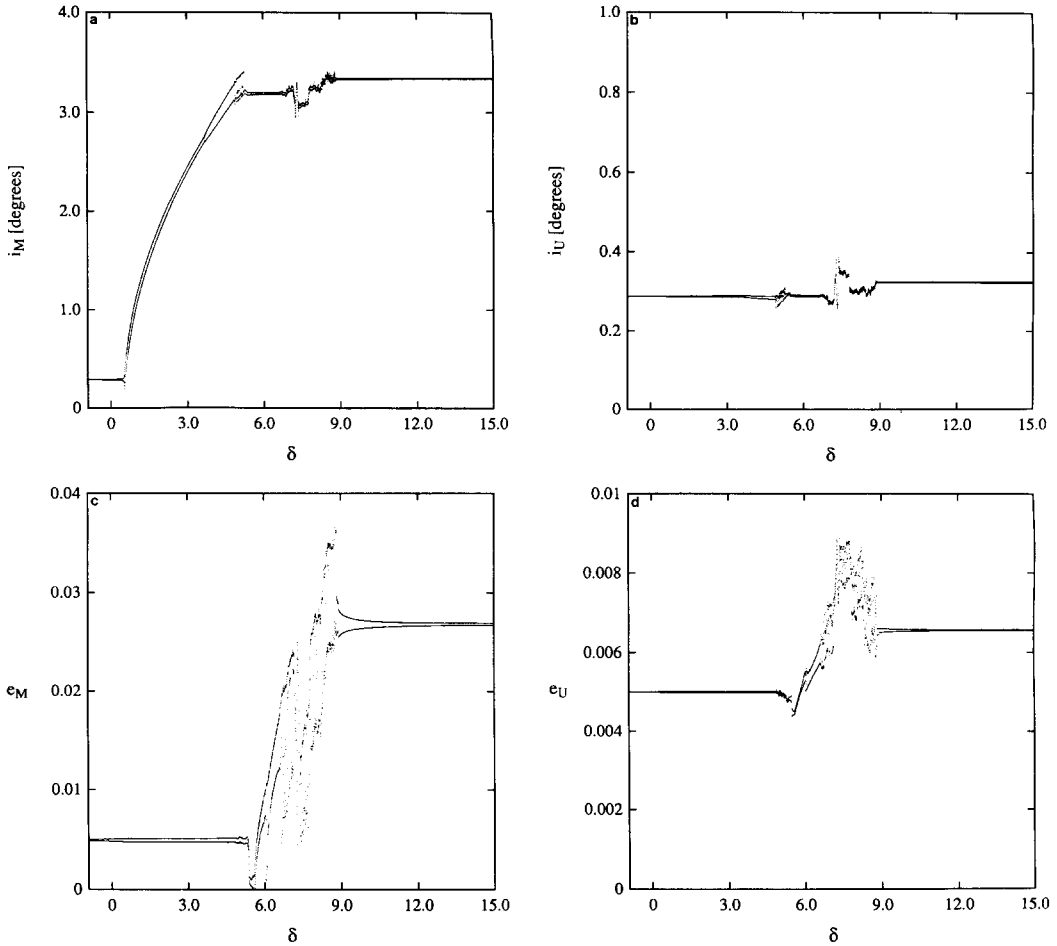
FIG. 18. Variations in the orbital inclinations (Miranda (a), Umbriel (b)) and eccentricities (Miranda (c), Umbriel (d)) of a trajectory evolved through the 3 : 1 Miranda–Umbriel mean-motion commensurability ($\dot{a}_M/a_M = 6 \times 10^{-12}$ per orbit period). The units of δ are year^{-1}. The inclination resonances are encountered first, and evolution within them is similar to the evolution in the circular-inclined approximation. There is a large chaotic zone associated with the eccentricity resonances. The orbital eccentricity of Miranda varies significantly within this chaotic zone, but the orbital inclination of Miranda remains high.

jectory further evolves, the oscillation amplitude of the orbital inclination of Miranda increases, while the mean orbital inclination of Umbriel decreases slightly. Between $\delta \approx 4.8$ and $\delta \approx 5.2$, the trajectory becomes chaotic. The trajectory shown in Fig. 18 escapes from the inclination resonances with average orbital inclinations of about $3°2$ for Miranda and about $0°28$ for Umbriel.

As the trajectory approaches the resonances, the amplitudes of oscillation of the

orbital eccentricities increase slightly. During the quasiperiodic phase of evolution through inclination resonance 1, the oscillation amplitudes of the orbital eccentricities are approximately constant until the trajectory becomes chaotic at $\delta \approx 4.8$, and then the eccentricities vary irregularly. After the trajectory escapes from the inclination resonances, the eccentricity resonances are encountered. At $\delta \approx 5.4$, the trajectory passes through the resonance involving

only the orbital pericenter of Umbriel (see Tittemore and Wisdom 1989). Between $\delta \approx 5.4$ and $\delta \approx 6.6$, the trajectory is mostly quasiperiodic, except for a burst of chaotic behavior at $\delta \approx 6$. The quasiperiodic phase is associated with temporary capture into the resonance involving both orbital pericenters (see Tittemore and Wisdom 1989). The trajectory eventually encounters a chaotic region associated with the eccentricity resonances. The relative variations of the eccentricities within the chaotic zone are large: the orbital eccentricity of Miranda oscillates irregularly between nearly zero and about 0.04, compared with the initial eccentricity of 0.005. The inclinations also vary chaotically, but the variations are not significant compared to the mean values, particularly for the orbit of Miranda. This trajectory eventually escapes from the eccentricity-type resonances, with an orbital eccentricity for Miranda of about 0.027 and an orbital eccentricity for Umbriel of about 0.0065. The final inclinations of the orbits do not change much: Miranda retains a high orbital inclination of about $3°4$. Other trajectories show similar behavior. The orbital eccentricity variations of Miranda within the chaotic region are larger if the orbital inclination of Miranda is high due to passage through the inclination resonances.

The orbital eccentricity variations of Miranda are spectacular, and e_M may reach a value of about 0.06 or higher before the satellites escape from the 3 : 1 commensurability. Tidal heating during this phase of the evolution may have had a significant effect on the thermal history of Miranda. This result is to be described in detail in a future paper (Tittemore and Wisdom 1989).

5. SECULAR PERTURBATIONS

In this section we consider the perturbations on the inclination-type resonances produced by the secular variations due to the other satellites. To get a qualitative idea of the effects of secular perturbations, we consider only the perturbations on the cir-

cular-inclined problem due to Ariel as a first approximation, since they are the most significant (see Dermott and Nicholson 1986, Laskar 1986). The development of the Hamiltonian is somewhat different, in order to keep secular variations distinct from resonant variations (see Wisdom 1982). If we define $\phi = \lambda_M - 3\lambda_U$, $p_i \approx i_i \sqrt{L_i} \cos(-\Omega_i)$, and $q_i \approx i_i \sqrt{L_i} \sin(-\Omega_i)$, and expand the Hamiltonian about the resonant value of L_M (pendulum approximation), then the momentum conjugate to ϕ is $\Phi = L_M - L_{MR}$. The Hamiltonian for the Miranda–Umbriel 3 : 1 resonance problem can then be expressed as

$$
\begin{aligned}
\mathcal{H} = {} & \tfrac{1}{2}\alpha\Phi^2 \\
& + C'(p_M^2 + q_M^2) + D'(p_U^2 + q_U^2) \\
& + E(p_M p_U + q_M q_U) \\
& + F((p_M^2 - q_M^2)\cos\phi + 2p_M q_M \sin\phi) \\
& + G((p_M p_U - q_M q_U)\cos\phi \\
& \quad + (p_M q_U + q_M p_U)\sin\phi) \\
& + H((p_U^2 - q_U^2)\cos\phi + 2p_U q_U \sin\phi),
\end{aligned}
\tag{38}
$$

where $\alpha \approx 32B$, and where C' and D' contain only secular contributions.

To include the perturbations due to Ariel, we add the terms in the disturbing function involving Ariel and its interactions with Miranda and Umbriel. We end up with the following expression for the Hamiltonian:

$$
\begin{aligned}
\mathcal{H} = {} & \tfrac{1}{2}\alpha\Phi^2 \\
& + C''(p_M^2 + q_M^2) + D''(p_U^2 + q_U^2) \\
& + E(p_M p_U + q_M q_U) \\
& + F((p_M^2 - q_M^2)\cos\phi + 2p_M q_M \sin\phi) \\
& + G((p_M p_U - q_M q_U)\cos\phi \\
& \quad + (p_M q_U + q_M p_U)\sin\phi) \\
& + H((p_U^2 - q_U^2)\cos\phi + 2p_U q_U \sin\phi) \\
& + U(p_A^2 + q_A^2) + V(p_M p_A + q_M q_A) \\
& + W(p_A p_U + q_A q_U).
\end{aligned}
\tag{39}
$$

The expressions for the coefficients $\alpha - W$ are given in Appendix 1.

In the units defined in Section 2, $m_M = 8.6 \times 10^{-7}$, $m_A = 1.55 \times 10^{-5}$, and $m_U = 1.47 \times 10^{-5}$ (Stone and Miner 1986). The
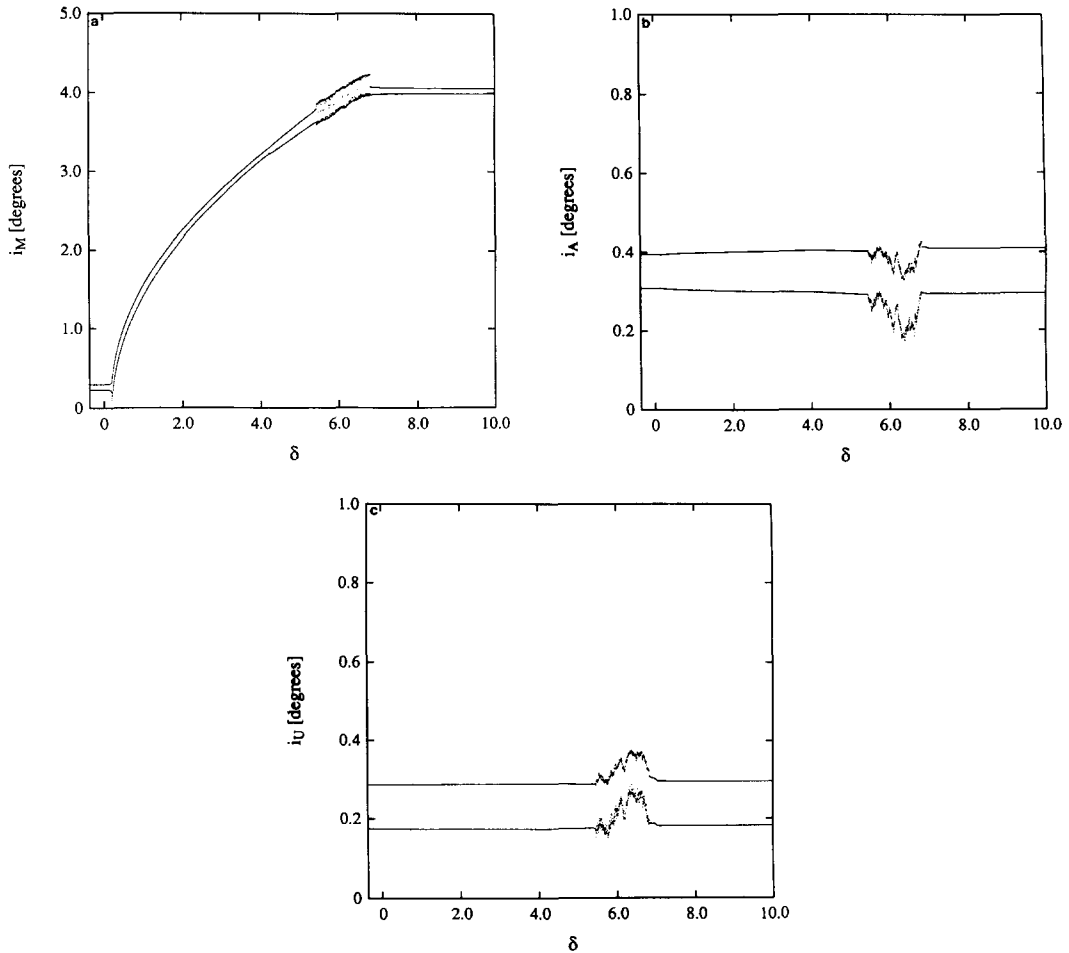
FIG. 19. Variations in the orbital inclinations of Miranda (a), Ariel (b), and Umbriel (c) for a trajectory perturbed by the secular variations of Ariel ($\dot{a}_M/a_M = 6 \times 10^{-12}$ per orbit period). The units of δ are year^{-1}. The variations in the orbital inclinations of Miranda and Umbriel are larger than those due only to their mutual perturbations. Again, the orbital inclination of Miranda increases considerably during temporary capture into resonance 1, and the orbital inclinations of the other satellites remain relatively unaffected by passage through the resonance.

numerical values of the coefficients are (see Appendix I): $\alpha = -165377.33$, $C'' = 0.189147$, $D'' = 0.0193986$, $E = -0.0006755$, $F = -0.0009763$, $G = 0.00039327$, $H = -0.0000396$, $U = 0.054396$, $V = -0.00451298$, and $W = -0.012133$. $L_{MR} = 0.033945497$.

We have derived a mapping for this Hamiltonian, analogous to the mapping derived by Wisdom (1982) to study the 3:1 Kirkwood gap. In this model, evolution due

to tidal dissipation changes the value of Φ at a rate of $\dot{L}_M = \frac{1}{2}L_{MR}(\dot{a}_M/a_M)$. The value of Φ can be converted into a value for δ.

Figure 19 shows the inclinations for a trajectory computed using this model. Away from the resonance, both the inclination of Miranda and the inclination of Umbriel are strongly perturbed by Ariel, resulting in much larger variations of the inclinations about the mean values than were found in the circular-inclined case. This trajectory is

captured into resonance 1. Again, there is a phase of quasiperiodic evolution within the resonance, during which various commensurabilities between the degrees of freedom are encountered. During this period, the amplitude of the variations in the orbital inclination of Ariel increases slightly, while the orbital inclination of Umbriel remains relatively unaffected. At $\delta \approx 4.2$, the trajectory encounters the 1 : 3 commensurability between the libration frequency and the frequency of circulation of σ_U. The trajectory is pulled into the chaotic zone at $\delta \approx 5.4$, and the inclinations of all three orbits vary chaotically until $\delta \approx 6.8$. The trajectory escapes from the resonance, leaving Miranda with an average orbital inclination of just over 4 degrees, and leaving the orbital inclinations of Ariel and Umbriel virtually unchanged.

Other trajectories show similar behavior. The presence of another degree of freedom provides a new set of secondary commensurabilities. The presence of Ariel complicates the structure of the resonance, and there appear to be resonant interactions involving the inclination of Ariel. However, the mechanisms that allow evolution to high orbital inclination for Miranda in the circular-inclined two-satellite approximation are still present in this model.

6. DISCUSSION

When Miranda and Umbriel encountered the 3 : 1 mean-motion commensurability, there was a significant probability that the system was captured into one of the inclination resonances involving the node of Miranda. Evolution within either of these resonances is described well by the single-resonance theory up to the point that the chaotic zone is encountered. The presence of this chaotic zone, along with the existence of commensurabilities between the libration frequencies and other fundamental frequencies in the system, allows the system to escape from the resonance with a high orbital inclination for Miranda. Since the timescale of damping of the inclinations

is long, this can explain Miranda's current high inclination. This is a significant new result, underscoring the importance of chaos in the dynamics of the solar system. The integrable theory of passage through isolated mean-motion resonances is useful up to a point, but it certainly cannot be used to predict the interesting features of the passage through this resonance. The interaction between resonances must be considered in order to adequately describe this problem.

The dynamical evolution of this problem is quite beautiful. Nonlinear dynamical systems have a self-similar structure at all scales (see, e.g., Hénon 1969), showing resonance within resonance within resonance, *ad infinitum*. The Miranda–Umbriel 3 : 1 mean-motion commensurability illustrates a physically important manifestation of this seemingly esoteric quality of dynamical systems: during evolution through the inclination resonances in this problem, trajectories will enter the chaotic zone in general only as a result of the slow evolution of the secondary resonances in phase space.

Since the mechanism described in this paper is a plausible explanation for the high orbital inclination of Miranda, the requirement that Miranda and Umbriel have passed through the 3 : 1 resonance also allows us to place an upper limit of 39,000 on the specific dissipation of Uranus (Q). The minimum value of Q which allows for reasonable evolution of the satellite system using the nominal masses of the satellites (see Stone and Miner 1986) is $Q = 6600$ (Peale 1988). However, we have found (Tittemore and Wisdom 1989) that permanent capture into the 2 : 1 mean-motion commensurability involving Ariel and Umbriel is very likely even if the orbital eccentricities approaching the resonance were considerably larger than their current values. It is therefore unlikely that the satellites ever encountered this resonance, further constraining the Q of Uranus to be greater than 11,000. Therefore, $11,000 \leq Q_U \leq 39,000$. The Ariel–Umbriel 2 : 1 commensurability will

be described in detail in an upcoming paper (Tittemore and Wisdom 1989).

We conclude that the current anomalously high orbital inclination of Miranda can be accounted for by temporary capture into the 3:1 resonance with Umbriel, and that it is therefore likely that the orbits of the satellites have tidally evolved at least enough to have allowed passage through this resonance.

7. APPENDIX I: AVERAGED RESONANT HAMILTONIAN COEFFICIENTS

7.1. Circular-Inclined Hamiltonian Coefficients

The expressions for the coefficients in the circular-inclined Hamiltonian (Eq. (9)) are

$$A = -\frac{1}{4}\frac{G^2M^2m_M^2m_M'}{\Gamma_M^3} + \frac{3}{4}\frac{G^2M^2m_U^2m_U'}{\Gamma_U^3}$$

$$B = -\frac{3}{32}\frac{G^2M^2m_M^2m_M'}{\Gamma_M^4} - \frac{27}{32}\frac{G^2M^2m_U^2m_U'}{\Gamma_U^4}$$

$$C = \frac{1}{2} G^4M^4R^2J_2 \left[\frac{9m_U^4m_U'^3}{2\Gamma_U^7}\right]$$
$$+ \frac{G^2Mm_Mm_U^2m_U'}{4\Gamma_U^2}\left[\frac{3}{\Gamma_U}b_{1/2}^0(\alpha)\right.$$
$$+ \frac{d}{d\alpha}b_{1/2}^0(\alpha)\frac{m_U}{m_M}\frac{m_U'}{m_M'}\left(\frac{\Gamma_M}{\Gamma_U^2} + \frac{3\Gamma_M^2}{\Gamma_U^3}\right)$$
$$\left. - \frac{(11)^{(0)}}{\Gamma_M}\right]$$

$$D = \frac{1}{2} G^4M^4R^2J_2 \left[\frac{6m_U^4m_U'^3}{\Gamma_U^7} - \frac{3m_M^4m_M'^3}{2\Gamma_M^7}\right]$$
$$+ \frac{G^2Mm_Mm_U^2m_U'}{4\Gamma_U^2}\left[\frac{3}{\Gamma_U}b_{1/2}^0(\alpha)\right.$$
$$+ \frac{d}{d\alpha}b_{1/2}^0(\alpha)\frac{m_U}{m_M}\frac{m_U'}{m_M'}$$
$$\left. + \left(\frac{\Gamma_M}{\Gamma_U^2} + \frac{3\Gamma_M^2}{\Gamma_U^3}\right) - \frac{(11)^{(0)}}{\Gamma_U}\right]$$

$$E = \frac{G^2Mm_Mm_U^2m_U'}{2\Gamma_U^2\sqrt{\Gamma_M\Gamma_U}}(11)^{(0)}$$

$$F = -\frac{G^2Mm_Mm_U^2m_U'}{4\Gamma_U^2\Gamma_M}(212)^{(3)}$$

$$G = \frac{G^2Mm_Mm_U^2m_U'}{2\Gamma_U^2\sqrt{\Gamma_M\Gamma_U}}(212)^{(3)}$$

$$H = -\frac{G^2Mm_Mm_U^2m_U'}{4\Gamma_U^3}(212)^{(3)}.\tag{40}$$

7.2. Eccentric-Inclined Hamiltonian Coefficients

The expressions for the coefficients $A - H$ in Eq. (37) are the same as those given above, with Γ_M and Γ_U defined in Section 4. The expressions for the coefficients $I - N$ in the Hamiltonian (Eq. (37)) are

$$I = \frac{1}{2} G^4M^4R^2J_2 \left[\frac{9m_U^4m_U'^3}{2\Gamma_U^7} - \frac{3m_M^4m_M'^3}{\Gamma_M^7}\right]$$
$$+ \frac{G^2Mm_Mm_U^2m_U'}{4\Gamma_U^2}\left[\frac{3}{\Gamma_U}b_{1/2}^0(\alpha)\right.$$
$$+ \frac{d}{d\alpha}b_{1/2}^0(\alpha)\frac{m_U}{m_M}\frac{m_U'}{m_M'}\left(\frac{\Gamma_M}{\Gamma_U^2} + \frac{3\Gamma_M^2}{\Gamma_U^3}\right)$$
$$\left. - \frac{(2)^{(0)}}{\Gamma_M}\right]$$

$$J = \frac{1}{2} G^4M^4R^2J_2 \left[\frac{3m_U^4m_U'^3}{\Gamma_U^7} - \frac{3m_M^4m_M'^3}{2\Gamma_M^7}\right]$$
$$+ \frac{G^2Mm_Mm_U^2m_U'}{4\Gamma_U^2}\left[\frac{3}{\Gamma_U}b_{1/2}^0(\alpha)\right.$$
$$+ \frac{d}{d\alpha}b_{1/2}^0(\alpha)\frac{m_U}{m_M}\frac{m_U'}{m_M'}$$
$$\left(\frac{\Gamma_M}{\Gamma_U^2} + \frac{3\Gamma_M^2}{\Gamma_U^3}\right) - \frac{(3)^{(0)}}{\Gamma_U}\right]$$

$$K = -\frac{G^2Mm_Mm_U^2m_U'}{4\Gamma_U^2\sqrt{\Gamma_M\Gamma_U}}(21)^{(-1)}$$

$$L = -\frac{G^2Mm_Mm_U^2m_U'}{4\Gamma_U^2\Gamma_M}(172)^{(3)}$$

$$M = -\frac{G^2Mm_Mm_U^2m_U'}{4\Gamma_U^2\sqrt{\Gamma_M\Gamma_U}}(182)^{(2)}$$

$$N = -\frac{G^2Mm_Mm_U^2m_U'}{4\Gamma_U^3}(192)^{(1)}\tag{41}$$

7.3. Secularly Perturbed Hamiltonian Coefficients

The expressions for the coefficients in the secularly perturbed circular-inclined Hamiltonian (Eq. (39)) are

$$\alpha = \frac{-3G^2M^2m_M^2m_M'}{L_M^4} - \frac{27G^2M^2m_U^2m_U'}{(L_U - 3L_M)^4}$$

$$C'' = \frac{3}{4}\frac{G^4M^4m_M^4m_M'^3R^2J_2}{L_M^7}$$
$$- \frac{G^2Mm_Mm_A^2m_A'}{4L_A^2}\frac{(11)_{MA}^{(0)}}{L_M}$$
$$- \frac{G^2Mm_Mm_U^2m_U'}{4L_U^2}\frac{(11)_{MU}^{(0)}}{L_M}$$

$$D'' = \frac{3}{4}\frac{G^4M^4m_U^4m_U'^3R^2J_2}{L_U^7}$$
$$- \frac{G^2Mm_Mm_U^2m_U'}{4L_U^2}\frac{(11)_{MU}^{(0)}}{L_U}$$
$$- \frac{G^2Mm_Am_U^2m_U'}{4L_U^2}\frac{(11)_{AU}^{(0)}}{L_U}$$

$$E = \frac{G^2Mm_Mm_U^2m_U'}{2L_U^2\sqrt{L_ML_U}}(11)_{MU}^{(0)}$$

$$F = -\frac{G^2Mm_Mm_U^2m_U'}{4L_U^2L_M}(212)_{MU}^{(3)}$$

$$G = \frac{G^2Mm_Mm_U^2m_U'}{2L_U^2\sqrt{L_ML_U}}(212)_{MU}^{(3)}$$

$$H = -\frac{G^2Mm_Mm_U^2m_U'}{4L_U^3}(212)_{MU}^{(3)}$$

$$U = \frac{3}{4}\frac{G^4M^4m_A^4m_A'^3R^2J_2}{L_A^7}$$
$$- \frac{G^2Mm_Mm_A^2m_A'}{4L_A^2}\frac{(11)_{MA}^{(0)}}{L_A}$$
$$- \frac{G^2Mm_Am_U^2m_U'}{4L_U^2}\frac{(11)_{AU}^{(0)}}{L_A}$$

$$V = \frac{G^2Mm_Mm_A^2m_A'}{4L_A^2\sqrt{L_ML_A}}(11)_{MA}^{(0)}$$

$$W = \frac{G^2Mm_Am_U^2m_U'}{4L_U^2\sqrt{L_AL_U}}(11)_{AU}^{(0)}.$$

ACKNOWLEDGMENT

REFERENCES

ALLAN, R. R. 1969. Evolution of Mimas–Tethys commensurability. *Astron. J.* **74**, 497–506.

ARNOLD, V. I. 1963. Small denominators and problems of stability of motion in classical and celestial mechanics. *Russian Math. Surveys* **18**, 85–91.

BORDERIES, N., AND P. GOLDREICH 1984. A simple derivation of capture probabilities for the $J + 1:J$ and $J + 2:J$ orbit–orbit resonance problems. *Celestial Mech.* **32**, 127–136.

BROUWER, D., AND G. M. CLEMENCE 1961. *Methods of Celestial Mechanics*. Academic Press, New York.

CHIRIKOV, B. V. 1979. A universal instability of many dimensional oscillator systems. *Phys. Rep.* **52**, 263–379.

COUNSELMAN, C. C., AND I. I. SHAPIRO 1970. Spin-orbit resonance of Mercury. *Symposia Mathematica* **3**, 121–169.

DARWIN, G. H. 1880. On the secular changes in the elements of the orbit of a satellite revolving about a tidally distorted planet. *Philos. Trans. Roy. Soc. London* **171**, 713–891.

DERMOTT, S. F. 1984. Origin and evolution of the Uranian and Neptunian satellites: Some dynamical considerations. In *Uranus and Neptune* (J. Bergstralh, Ed.), NASA Conference Publication 2330, pp. 377–404.

DERMOTT, S. F., AND P. D. NICHOLSON 1986. Masses of the satellites of Uranus. *Nature* **319**, 115–120.

FRENCH, R. G., J. L. ELLIOT, AND S. L. LEVINE 1985. Structure of the Uranian rings. II. Perturbations of the ring orbits and widths. *Icarus* **67**, 134–163.

GOLDREICH, P. 1965. An explanation of the frequent occurrence of commensurable mean motions in the solar system. *Mon. Not. Roy. Astron. Soc.* **130**, 159–181.

GOLDREICH, P., AND S. J. PEALE 1966. Spin-orbit coupling in the Solar System. *Astron. J.* **71**, 425–438.

HÉNON, M. 1969. Numerical study of quadratic area-preserving mappings. *Quart. Appl. Math.* **26**, 291–311.

HÉNON, M., AND C. HEILES 1964. The applicability of the third integral of motion: Some numerical experiments. *Astron. J.* **69**, 73–79.

HENRARD, J. 1982. Capture into resonance: an extension of the use of adiabatic invariants. *Cel. Mech.* **27**, 3–22.

HENRARD, J., AND A. LEMAITRE 1983. A second fundamental model for resonance. *Celestial Mech.* **30**, 197–218.

KAULA, W. M. 1964. Tidal dissipation by solid friction and the resulting orbital evolution. *Rev. Geophys.* **2**, 661–685.

LASKAR, J. 1986. A general theory for the Uranian satellites. *Astron. Astrophys.* **166**, 349–358.

LEMAITRE, A. 1984. High-order resonances in the restricted three-body problem. *Celestial Mech.* **32**, 109–126.

LEVERRIER, U.-J. 1855. Développement de la fonction qui sert de base au calcul des perturbations des mouvements des planètes. *Ann. Obs. Paris, Mém.* **1**.

MACDONALD, G. J. F. 1964. Tidal friction. *Rev. Geophys.* **2**, 467–541.

PEALE, S. J. 1976. Orbital resonances in the Solar System. *Annu. Rev. Astron. Astrophys.* **14**, 215–245.

PEALE, S. J. 1986. Orbital resonances, unusual configurations, and exotic rotation states among planetary satellites. In *Satellites* (J. Burns and M. Matthews, Eds.), pp. 159–223. Univ. of Arizona Press, Tucson.

PEALE, S. J. 1988. Speculative histories of the Uranian satellite system. *Icarus* **74**, 153–171.

PLUMMER, H. C. 1960. *An Introductory Treatise on Dynamical Astronomy*. Dover, New York.

SINCLAIR, A. T. 1972. On the origin of the commensurabilities amongst the satellites of Saturn. *Mon. Not. Roy. Astron. Soc.* **160**, 169–187.

SINCLAIR, A. T. 1974. On the origin of the commensurabilities amongst the satellites of Saturn, II. *Mon. Not. Roy. Astron. Soc.* **166**, 165–179.

SMITH, B. A., L. A. SODERBLOM, R. BEEBE, D. BLISS, J. M. BOYCE, A. BRAHIC, G. A. BRIGGS, R. H. BROWN, S. A. COLLINS, A. F. COOK II, S. K. CROFT, J. N. CUZZI, G. E. DANIELSON, M. E. DAVIES, T. E. DOWLING, D. GODFREY, C. J. HANSEN, C. HARRIS, G. E. HUNT, A. P. INGERSOLL, T. V. JOHNSON, R. J. KRAUSS, H. MASURSKY, D. MORRISON, T. OWEN, J. B. PLESCIA, J. B. POLLACK, C. C. PORCO, K. RAGES, C. SAGAN, E. M. SHOEMAKER, L. A. SROMOVSKY, C. STOKER, R. G. STROM, V. E. SUOMI, S. P. SYNNOTT, R. J. TERRILE, P. THOMAS, W. R. THOMPSON, AND J. VEVERKA 1986. Voyager 2 in the Uranian system: Imaging science results. *Science* **233**, 43–64.

SQUYRES, S. W., R. T. REYNOLDS, AND J. J. LISSAUER 1985. The enigma of the Uranian satellites' orbital eccentricities. *Icarus* **61**, 218–233.

STONE, E. C. AND E. D. MINER 1986. The Voyager 2 encounter with the Uranian system. *Science* **233**, 39–43.

TITTEMORE, W. C. 1988. *Tidal Evolution of the Uranian Satellites*. Ph.D. thesis, Massachusetts Institute of Technology.

TITTEMORE, W. C., AND J. WISDOM 1988. Tidal evolution of the Uranian satellites. I. Passage of Ariel and Umbriel through the 5:3 mean-motion commensurability. *Icarus* **74**, 172–230.

TITTEMORE, W. C., AND J. WISDOM 1989. Tidal evolution of the Uranian satellites. III. Evolution through the Miranda–Umbriel 3:1, Miranda–Ariel 5:3, and Ariel–Umbriel 2:1 mean-motion commensurabilities. Submitted for publication.

VEILLET, C. 1983. *De l'observation et du mouvement des satellites d'Uranus*. Thèse de Doctorate d'Etat, Université de Paris.

WISDOM, J. 1980. The resonance overlap criterion and the onset of stochastic behavior in the restricted three-body problem. *Astron. J.* **85**, 1122–1133.

WISDOM, J. 1982. The origin of the Kirkwood gaps: A mapping for asteroidal motion near the 3/1 commensurability. *Astron. J.* **87**, 577–593.

WISDOM, J. 1983. Chaotic behavior and the origin of the 3/1 Kirkwood gap. *Icarus* **56**, 51–74.

WISDOM, J. 1985a. A perturbative treatment of motion near the 3/1 commensurability. *Icarus* **63**, 272–289.

WISDOM, J. 1985b. Meteorites may follow a chaotic route to Earth. *Nature* **315**, 731–733.

WISDOM, J. 1987. Chaotic dynamics in the Solar System. *Icarus* **72**, 241–275.

YODER, 1979. Diagrammatic theory of transition of pendulum-like systems. *Celestial Mech.* **19**, 3–29.